# *NAVIER-STOKES SIMULATION OF THE CROSSFLOW INSTABILITY IN SWEPT-WING FLOWS*

A Final Report To

National Aeronautics and Space Administration
Langley Research Center
Hampton, Virginia 23665

NAG1-874

October 1989

Submitted by

HELEN L. REED

Department of Mechanical and Aerospace Engineering
College of Engineering and Applied Science
Arizona State University
Tempe, AZ 85287-6106

John K. Burchard, Ph.D.
Assistant Director,
Office of Research Development & Administration
(602) 965-2170

## ABSTRACT

Here we describe the computational modeling of the transition process characteristic of flows over swept wings. Specifically, the crossflow instability and crossflow/T-S wave interactions are analyzed through the numerical solution of the full three-dimensional Navier-Stokes equations including unsteadiness, curvature, and sweep. This approach is chosen because of the complexity of the problem and because it appears that linear stability theory is insufficient to explain the discrepancies between different experiments and between theory and experiments (e.g., steady vs. unsteady, interactions, . . .). The leading edge region of a swept wing is considered in a three-dimensional *spatial* simulation with random disturbances as the initial conditions.

The work has been closely coordinated with the experimental program of Professor William Saric, also at Arizona State University, examining the same problem. Comparisons with NASA flight test data and the experiments at Arizona State University were a necessary and an important integral part of this work.

TABLE OF CONTENTS

## 1. INTRODUCTION

This final report describes the research program previously funded under NASA Grants NAG-1-731 and NAG-1-874. After October 4, 1989, this work has been unfunded.

In this report, Section 2 contains a list of related experience and accomplishments associated with this effort. Section 3 contains a summary of the completed work using a spatial, full Navier-Stokes simulation to examine the crossflow instability on swept wings. The resources and personnel involved in this project are described in Section 5.

## 2. RELATED EXPERIENCE AND TECHNICAL ACCOMPLISHMENTS

In the past 7 years, 7 students were supervised, 17 publications were written, and 29 talks and lectures were given.

*Publications*

1. "Wave Interactions in Swept-Wing Flows," H.L. Reed, *AIAA Paper 84-1678.*
2. "Report of Computational Group," H.L. Reed, in *Transition in Turbines,* NASA CP 2386, NASA Lewis Research Center, May 1984.
3. "An Analysis of Wave Interactions in Swept-Wing Flows," H.L. Reed, 2nd IUTAM Symposium on *Laminar-Turbulent Transition*, ed. V.V. Kozlov and V. Ya Levchenko, Springer-Verlag, New York, 1985.
4. "Disturbance-Wave Interactions in Flows with Crossflow," H.L. Reed, *AIAA Paper 85-0494.*
5. "Wave Interactions in Swept-Wing Flows," H.L. Reed, *Phys. Fluids*, Vol. 30, No. 11, p. 3419, 1987.
6. "Stability and Transition of Three-Dimensional Flows," H.L. Reed and W.S. Saric, *Invited Paper*, in *Proceedings of the Tenth U.S. National Congress of Applied Mechanics*, ASME, New York, 1987.
7. "Three-Dimensional Stability of Boundary Layers," W.S. Saric and H.L. Reed, in *Perspectives in Turbulence Studies*, ed. H.U. Meier and P. Bradshaw, Springer-Verlag, New York, 1987.
8. "Stability of Three-Dimensional Boundary Layers," H.L. Reed, *Invited Paper*, SAE 871857, AEROTECH '87 (Aerospace Technology Conference and Exposition), Long Beach, Oct. 5-8, 1987.
9. "Stability and Transition of Three-Dimensional Boundary Layers," W.S. Saric and H.L. Reed, *Invited Paper*, AGARD Conference No. 438, *Fluid Dynamics of*

*Three-Dimensional Turbulent Shear Flows and Transition*, Cesme, Turkey, Oct. 1988.

10. "Stability of Three-Dimensional Boundary Layers," H.L. Reed and W.S. Saric, *Ann. Rev. Fluid Mech.*, Vol. 21, p. 235, 1989.

11. "Supersonic/Hypersonic Laminar/Turbulent Transition," H.L. Reed, G.K. Stuckert, and P. Balakumar, *Invited Paper*, in *Developments in Mechanics*, Vol. 15, Proceedings of the 21st Midwestern Mechanics Conference, Aug. 13-16, 1989.

12. "Receptivity of the Boundary Layer on a Semi-Infinite Flat Plate with an Elliptic Leading Edge," N. Lin, H.L. Reed, and W.S. Saric, Arizona State University, ASU 90006, Sept. 1989.

13. "Boundary-Layer Receptivity: Computations," N. Lin, H.L. Reed, and W.S. Saric, Third International Congress of Fluid Mechanics, Cairo, Egypt, January 2-4, 1990.

14. "Stability of High-Speed Chemically Reacting and Three-Dimensional Boundary Layers," H.L. Reed, G.K. Stuckert, and P. Balakumar, 3rd IUTAM Symposium on *Laminar-Turbulent Transition*, ed. R. Michel and D. Arnal, Springer-Verlag, New York, to be published, 1990.

15. "Stability of Three-Dimensional Supersonic Boundary Layers," P. Balakumar and H.L. Reed, submitted to *Phys. Fluids*.

16. "A Shear-Adaptive Solution of the Spatial Stability of Boundary Layers with Outflow Conditions," H. Haj-Hariri and H.L. Reed, in preparation.

17. "Spatial Simulation of Boundary-Layer Transition," H.L. Reed, *Invited paper*, in preparation for *Appl. Mech. Rev.*

*Presentations*

1. "Boundary Layer Stability - Recent Developments," H.L. Reed, Seminar in Fluid Mechanics, Nov. 2, 1982, Stanford.

2. "An Analysis of Instabilities in Laminar Viscous Flows," H.L. Reed, *Invited Seminar* in Applied Mathematics, Sandia National Laboratories, Albuquerque, Aug. 3, 1983.

3. "Wave Interactions in Swept-Wing Flows," H.L. Reed, NASA/Langley Research Center, June 13, 1984.

4. "Wave Interactions in Swept-Wing Flows," H.L. Reed, *Invited Paper*, 21st Annual Meeting of the Society of Engineering Science, Inc., VPI&SU, Blacksburg, Oct. 15-17, 1984.

5. "Crossflow/Tollmien-Schlichting Interactions in Swept-Wing Flows," H.L. Reed, Bull. Amer. Phys. Soc., Vol. 29, No. 9, p. 1554, Nov. 1984.

6. "Disturbance-Wave Interactions in Flows with Crossflow," H.L. Reed, *Invited*, Fluid Mechanics Seminar, UC Berkeley, Feb. 28, 1985.

7. "Computational Simulation of Transition," H.L. Reed, ICASE Meeting of Stability Theory, NASA/Langley Research Center, Nov. 21, 1986.

8. "Stability and Transition of Three-Dimensional Flows," H.L. Reed and W.S. Saric, *Invited Seminar*, Princeton, Apr. 21, 1987.

9. "Three-Dimensional Boundary-Layer Stability," H.L. Reed, *Invited Lecture*, Univ Ore, Eugene, Nov. 6, 1987.

10. "Three-Dimensional Boundary-Layer Stability," H.L. Reed, *Invited Talk*, Naval Post Graduate School, Monterey, Feb. 18, 1988.

11. "Computational Simulation of Three-Dimensional Boundary-Layer Flows," H.L. Reed, *Invited Lecture*, Tohoku University, Sendai, Japan, Apr. 1988.

12. "Computational Simulation of Three-Dimensional Boundary-Layer Flows," H.L. Reed, *Invited Lecture*, Hokkaido University, Sapporo, Japan, Apr. 1988.

13. "Energy-Efficient Aircraft," H.L. Reed, *Invited Talk*, Society of Women Engineers, Notre Dame, Nov. 9, 1988.

14. "Three-Dimensional Boundary-Layer Stability," H.L. Reed, *Invited Talk*, IBM Lecture Series, Notre Dame, Nov. 9, 1988.

15. "A Shear-Adaptive Approach to Spatial Simulations of Transition," H. Haj-Hariri and H.L. Reed, Bull. Amer. Phys. Soc., Vol. 33, No. 10, Nov. 1988.

16. "Three-Dimensional Boundary-Layer Stability," H.L. Reed, *Invited Lecture*, University of Western Ontario, London, Canada, Nov. 23, 1988.

17. "Three-Dimensional Boundary-Layer Stability," H.L. Reed, *Invited Seminar*, Univ Houston, Mar. 2, 1989.

18. "Boundary-Layer Receptivity: Computations," N. Lin, H.L. Reed, and W.S. Saric, Bull. Amer. Phys. Soc., Vol. 34, No. 10, Nov. 1989.

*Post Doctoral Associates*

H. Haj-Hariri, "Spatial Simulation of Transition," completed Spring 1988.

P. Balakumar, "Stability of Three-Dimensional Supersonic Boundary Layers," completed Spring 1989.

*Ph.D. Students*

R.S. Lin, "The Crossflow Instability in Swept-Wing Flows," expected Spring 1991.

N. Lin, "Boundary-Layer Receptivity," expected Spring 1992.

T. Buter, "Boundary-Layer Receptivity to Three-Dimensional Disturbances," expected Spring 1992.

*MS Students*

N. Lin, "Receptivity of the Boundary-Layer Flow over a Semi-Infinite Flat Plate with an Elliptic Leading Edge," completed Fall 1989.

*Undergraduate Students*

T. Haynes, "Stability of Boundary-Layer Flows," completed Fall 1988.

G. Loring, "Secondary Instabilities in Three-Dimensional Boundary Layers," completed Summer 1989.

Most of the technical accomplishments thus far are documented in the publications listed above. A brief description follows.

"Wave Interactions in Swept-Wing Flows," H.L. Reed, *Phys. Fluids*, Vol. 30, No. 11, p. 3419, 1987. Secondary-instability theory for three-dimensional boundary layers is described. In particular, it is shown that the early crossflow experiments of Saric exhibited a resonance between the fundamental and the second harmonic.

"Stability of Three-Dimensional Boundary Layers," H.L. Reed and W.S. Saric, *Ann. Rev. Fluid Mech.*, Vol. 21, p. 235, 1989. The paper is a complete literature review of the area of three-dimensional boundary-layer stability and transition as of June 1988. It obviates the need to review the literature in this final report.

"A Shear-Adaptive Solution of the Spatial Stability of Boundary Layers with Outflow Conditions," H. Haj-Hariri and H.L. Reed, in preparation. This work outlines the numerics and boundary conditions used in our spatial simulations of transition.

"Stability of Three-Dimensional Boundary Layers," H.L. Reed, *Invited Paper*, SAE 871857, AEROTECH '87 (Aerospace Technology Conference and Exposition), Long Beach, Oct. 5-8, 1987. Here our computational simulations of swept wing flows are described, with results presented for the basic state.

"Stability of Three-Dimensional Supersonic Boundary Layers," P. Balakumar and H.L. Reed, submitted to *Phys. Fluids*. Provides the characteristics of crossflow in supersonic flow.

"Receptivity of the Boundary Layer on a Semi-Infinite Flat Plate with an Elliptic Leading Edge," N. Lin, H.L. Reed, and W.S. Saric, Arizona State University Report CEAS 90006, Sept. 1989. This report demonstrates the feasibility of numerically studying the receptivity problem and establishes the platform upon which our receptivity studies are based. This work represents the first successful numerical treatment of the receptivity problem!

The basic accomplishments of our efforts to study the crossflow instability thus far can be outlined as follows:

1. General, three-dimensional spatial stability code developed with curvature to support the experiments and the computations

2. Secondary-instability theory developed for swept-wing flows. The second haromonic was identified to explain the experiments of Saric.

3. Streakline calculator developed to visualize the structures predicted by the theory.

4. Full Navier Stokes, spatial-simulation numerics developed.

5. Two-dimensional basic-state flow over an elliptic-nosed flat plate established including leading edge and curvature using full Navier Stokes.

6. Three-dimensional basic state flow over a swept wing established including leading edge and curvature using full Navier Stokes.

7. Two-dimensional disturbance flow over an unswept wing established including leading edge and curvature using full Navier Stokes.

8. Correlated results of #7 with stability theory of #1.

9. Three-dimensional basic state and unsteady disturbance field for flow over a swept curved-leading-edge/thick-flat-plate combination including curvature.

10. Freestream disturbance field established for initial/boundary conditions for receptivity studies.

11. Established platform for receptivity studies for unswept wing.

12. Established the characteristics of crossflow in supersonic flow using a rotating-cone model.

## 3. DESCRIPTION OF THE COMPUTATIONS

Direct numerical simulations are playing an increasingly important role in the investigation of transition. In such simulations, the full Navier-Stokes equations are solved directly by employing numerical methods, such as finite-difference or spectral methods. This approach is widely applicable since it avoids many of the restrictions that usually have to be imposed in theoretical models. From recent developments, it is apparent that linear stability theory suffers from this; the discrepancies between theory and experiment (i.e. steady versus unsteady; the role of interactions; the role of roughness, curvature, and freestream disturbances) are currently unexplainable for crossflow. It appears that stability theory is not well-posed; predicted N-factors can range from small to large for a given configuration depending on the version of theory used (e.g. Collier and Malik 1989 and Collier et al. 1989). The questions posed above must be addressed by computational simulations.

In this approach, in contrast to linear stability theory, no restrictions with respect to the form or amplitude of the disturbances have to be imposed, because no linearizations or special assumptions concerning the disturbances have to be made. Furthermore, this approach allows the realistic treatment of the space-amplified disturbances and no assumptions have to be made concerning the basic flow (such as that the flow be parallel). The basic idea of this method is to disturb an established basic flow by forced, time-dependent perturbations. Then the reaction of this flow, that is, the temporal and spatial development of the perturbations, is determined by the numerical solution of the complete Navier-Stokes equations.

The principal goal of the current research is therefore the *spatial* simulation of the process of laminar-turbulent transition in the leading-edge region of an infinitely long, swept wing. The existence of such a method will provide a tool which will enable computation to complement experimental contributions to further the understanding of the physics of these flows and, ultimately, will provide a tool for the prediction and modeling of these flows. This is an ambitious goal.

The first issue was the choice of flow to be modeled. The domain of interest was the leading edge region of a swept wing, extending back into the flat-pressure region to allow interactions between T-S waves and crossflow vortices to occur and be studied. Initially, the configuration considered was one with surface curvature, e.g. a swept flat plate with an elliptical nose; this was termed Configuration 1. When confidence and basic understanding are gained in the modeling of this basic flow, then we could begin to study an actual Laminar Flow Control (suction) and/or Natural Laminar Flow (pressure-gradient tailoring) configuration. In particular, a 45°-swept, NLF(2)-0415 airfoil at a

chord Reynolds number of 2.5 million could be used. There is an advantage to studying this shape, since this is the model in the ongoing experiments of Saric at ASU and, therefore, direct comparisons and predictions are possible. This is termed Configuration 2.

The approach used was the numerical solution of the full, unsteady, incompressible Navier-Stokes equations, including curvature, in the semi-infinite space above the leading-edge region of a wing. The success of previous investigators (Fasel 1980, Orszag and Kells 1980, Kleiser and Schumann 1984, Hussaini and Zang 1987) showed that this technique was not only feasible and an attractive complement to experiments, but was also informative because it was possible to have complete control of both initial and boundary conditions.

We have successfully completed the three-dimensional basic state and unsteady disturbance flow field. The leading-edge region of the flow field is characterized by very large streamwise velocity gradients such that the boundary-layer approximation cannot be made. Solutions of the complete Navier-Stokes equations including curvature are required to obtain the details of the flow. In the present study, the equations are written in a body-fitted orthogonal coordinate system so that arbitrary geometries can be treated. A conformal (Schwarz-Christoffel) mapping transforms the 2-D-cross-section of the swept surface to a straight line in a semi-infinite plane, and the 2-D component of the flow is solved in a 2-D rectangular computational domain for freestream speed $U_\infty \cos\Lambda$ ($U_\infty$ is the 3-D freestream speed and $\Lambda$ is the sweep angle). The formulation is directly extendable to three-dimensional flows under the conical flow assumption $\partial p/\partial z = 0$, where z lies along the root of the wing.

The computational box, with upstream end close to the leading edge and downstream end in the zero-pressure-gradient region in mid-chord, is fixed to the surface. The boundary conditions used correspond to no-slip and no-penetration (except when local suction/blowing is applied) at the wall, inviscid-flow conditions far away from the body, and convective conditions (*used in conjunction with the ideas of Macaraeg and Streett)* on the downstream boundary. For the disturbance state, the upstream condition is random unsteady noise.

For the disturbance state, we used Fourier methods and periodic boundary conditions in the spanwise direction (direction parallel to the leading edge) only; this assumption appeared to be totally justified from past stability analyses for this basic state, an infinite nontapered swept wing for which $\partial p/\partial z = 0$. We used finite-difference methods in the other two orthogonal directions. The basic methods are well developed. We resolved the disturbance field with an appropriate time differencing scheme to insure

numerical stability and adequately capture time-dependent behavior. Throughout, we determine and monitor resolution requirements, box size, and validity of the assumptions used.

At present we have successfully completed the grid generation and the solution of the

1. Two-dimensional basic state and unsteady disturbance field including the leading edge and curvature. See the next section and Figures 1-20. Also for disturbances introduced at the leading edge, see Figures 24-30.

2. Three-dimensional basic state (that is, the basic flow over the swept wing) including the leading edge and curvature. Typical results of pressure distribution and streamwise and crossflow velocity are shown in Figures 21-23.

3. Three-dimensional unsteady disturbance field for flow over a swept curved-leading-edge/thick-flat-plate combination including curvature. Results are in preparation.

Now that the platform is established, the next logical step for this work is to catalogue the time and spatial evolution of an instability added to the mean flow at the leading edge as an initial condition. Here, we would use various three-dimensional, unsteady, low-amplitude disturbances, including the case of random white noise which eliminates the possibility of bias from the researcher. We now have the capability to study the following issues:

1. Steady versus unsteady crossflow
2. The role of interactions
3. The role of sweep and curvature
4. The role of linear stability theory

We would conduct calculations of stability behavior and qualitatively compare with experimental results and with previous calculation schemes. We would evaluate the roles of unsteadiness, interactions, and parameters such as sweep angle and leading-edge radius. We would visualize flow structures associated with the transition process.

Furthermore, we would include wall suction and apply the techniques and results to typical LFC and NLF situations. In particular, comparisons (including N-factor calculations) would be made with the detailed, companion experiments of Saric also at ASU on the 45°-swept NLF(2)-0415 airfoil.

In addition, we would study receptivity, that is, the effects of various initial conditions/freestream boundary conditions. Since we are using a full spatial simulation, this important work is possible and has been demonstrated to be feasible, as shown in the ASU Report CRR 90006 "Receptivity of the Boundary Layer over a Semi-Infinite Flat Plate with an Elliptic Leading Edge." Results are presented in the next section. This

effort would support the NASA/Langley flight tests in determining whether engine noise is a factor, or not, in the transition process.

The work has been closely coordinated with experimental programs also at ASU, which are examining the same problem. Comparisons with NASA flight-test data and the experiments at ASU (including N-factor calculations) have always been considered necessary and an important integral part of this work.

## 4. RELATED RECEPTIVITY RESULTS

Boundary-layer receptivity has been discussed in many different forms (Morkovin, 1978, 1983; Mack, 1977; Tani, 1980; to name a few) and has been distinguished by remaining quite opaque. In fact, it is difficult to diagnose whether too little effort has been expended or too little success has been made. However, transition to turbulence will never be successfully understood without answering this fundamental problem (Saric, 1985). The basic question is how freestream turbulence and acoustic signals enter the boundary layer and ultimately generate unstable T-S waves. There is no simple or direct manner for this to happen except in the case of acoustic waves incident on supersonic boundary layers (Mack, 1977). It has long been speculated that the mechanism for freestream disturbances to enter the boundary layer is through the leading-edge region. In this regard, the asymptotic analysis of Goldstein (1983a, 1983b) is encouraging in that it appears to be the first step in analyzing the leading-edge/acoustic-wave problem. The recent experimental work of Leehey and Shapiro (1980) and Gedney (1983) did not focus on the leading edge, and their results have not been completely conclusive. The recent work is summarized by Reshotko (1984) and Goldstein and Hultgren (1989). There is a definite need to continue work in this area with an infusion of new ideas and techniques.

In our work, the receptivity of a flat-plate boundary layer to freestream disturbances is being investigated through the numerical solution of the Navier-Stokes equations in the leading-edge region. By stipulating the plate to have finite curvature at the leading edge (a feature left out of some unsuccessful receptivity models), the singularity there is removed and a new length scale is introduced. The particular geometry chosen is a semi-ellipse joined to a flat plate. The Reynolds number, based on leading edge curvature, is varied parametrically along with the aspect ratio of the ellipse in order to examine the stability of a wide variety of basic states. The use of various aspect ratios covers the range from a sharp leading edge to a semi-circular leading edge to a blunt leading edge.

The main feature of the numerical work here is the use of a body-fitted curvilinear coordinate system to calculate the flow at the elliptic leading-edge region with fine resolution. First, a basic-state solution is obtained by solving the governing equations for steady, incompressible flow with a uniform freestream using a transient approach. Then the basic flow is disturbed by applying time-dependent, forced perturbations as unsteady boundary conditions. The unsteady flow and the temporal and spatial development of the perturbations are determined by numerically solving the unsteady governing equations time accurately. An implicit finite-difference method is used in the streamwise and

normal directions and in time, while the spanwise direction is resolved by Fourier series. No artificial diffusion is used, yet the numerical methods are found to be robust and stable with the use of reasonably small time steps.

## 4.1 BASIC-STATE RESULTS

As preliminary results for presentation here, basic-state solutions for steady flow over a semi-infinite flat plate are obtained for two test cases. In calculations, the minor radius of the ellipse is used as a reference length L. The first case corresponds to a rather blunt leading edge with aspect ratio (AR; ratio of major to minor axes) of 3; the second case to a relatively sharp leading edge with aspect ratio 9. See Figures 1 and 2. In both cases, the Reynolds number based on reference length is 2400. The length of the flat plate at the downstream end of the computational box measured from the tip of the ellipse is 45L. The farfield boundary is located at 36L which is 36 times the plate thickness or about 30 times the Blasius boundary-layer thickness at the downstream boundary.

The steady-state flow solutions are obtained in a transient approach with a nondimensional $\Delta t$ of 0.007 X AR for the first case AR = 3 and a smaller value of $\Delta t$ of 0.0008 X AR for AR = 9. Altogether, 136 grid points are used in the streamwise direction with approximately 10 grid points in the expected T-S wavelength. In the normal direction 80 grid points are used. In both cases, the grid is stretched such that there are approximately 15 grid points in the boundary layer at the ellipse-flat-plate juncture. The convergence criteria was set as $10^{-8}$ for maximum residual and absolute error in vorticity and velocity between two time-iteration steps.

Velocity vectors are shown for the two cases in Figures 3 and 4. The velocity vector profiles obtained near the leading edge have some overshoot of the freestream value due to the acceleration over the convex curvature, the overshoot being more pronounced with the blunt leading edge. These profiles verify that solutions obtained by using the boundary-layer assumption or the infinitely sharp flat-plate assumption are missing vital information at the leading edge and are not valid for actual leading edges with finite thickness. The profiles gradually approach profiles with a slight adverse pressure gradient downstream.

Corresponding vorticity profiles at different streamwise locations are shown in Figures 5 and 6. Inflection points are clearly present at the leading-edge region. The pressure gradient along the wall is related to the normal gradient of vorticity at the wall and is shown in Figures 7 and 9. Surface pressure coefficient ($C_p$) is then obtained by integrating this expression along the wall; this is shown in Figures 8 and 10 along with

the corresponding inviscid $C_p$ obtained by a linear surface-panel method. The effect of leading-edge bluntness is illustrated in these figures. The blunt AR = 3 leading edge has a sharp peak (minimum) in surface pressure before recovering rapidly to the freestream pressure and approaching zero pressure gradient. The sharp leading edge has a more rapid approach to the minimum which is smaller (in magnitude) than the minimum in the blunt case. Both surface pressure distributions are close to the inviscid solution except in the rapid pressure-recovery region near the leading edge.

Wall vorticity distributions for the two cases are displayed in Figures 11 and 12. The maximum wall vorticity is 61.9 for the AR = 3 case and occurs at x = 0.12 at the leading edge. For the AR = 9 case, the maximum is 80.5 and occurs at x = 0.09. At the leading edge, the wall vorticity exhibits singularity-like behavior, which is found to be stronger for the AR = 9 case. The blunt case vorticity has a minimum near the leading edge, indicating an approach to separation, but no apparent minimum is observed for the sharp case. Wall vorticity predicted by the boundary-layer assumption underestimates the downstream value.

Another important parameter in presenting the steady flow results is the displacement thickness. Since velocity overshoots occur at the leading edge, the freestream velocity at the boundary-layer edge required in the integration is taken to be the maximum tangential velocity. The nondimensional displacement thickness $\delta^*$ should vary as $x^{1/2}$ according to boundary-layer theory. $\delta^{*2}$ obtained in the present calculation is plotted as a function of x in Figures 13 and 14 and clearly demonstrates the above linear behavior in the downstream region. $\delta^*$ is zero at the stagnation point, remains small in the favorable pressure-gradient region, and rises rather rapidly in the pressure recovery region where the boundary layer thickens. By linear continuation, the location of the virtual leading edge can be approximated. The virtual leading edge occurs at x = -6.0 for AR = 3 and at x = -1.8 for AR = 9; the virtual leading edge approaches the actual one as the leading edge sharpens.

## 4.2 UNSTEADY-DISTURBANCE RESULTS

Two cases are complete, demonstrating the ability of the present numerical method to perform unsteady time-accurate calculations to simulate receptivity to freestream fluctuations. Both calculations were performed on the AR = 3 flat plate, with the unsteady boundary conditions applied at the farfield being small time-harmonic oscillations of the streamwise velocity with amplitude $10^{-4}$, well in the linear range and of the same order of the amplitudes used by Saric in his recent experiments.

In case (1), the oscillations of the freestream streamwise velocity have dimensionless frequency parameter F = 333 (= $2 \pi \nu f / U_\infty^2 \times 10^6$). Perturbations that eventually develop in the flow will vary at constant forcing frequency, thus following F = constant lines with downstream distance. For F = 333, this line passes above the instability loop according to linear parallel-flow theory (in the stable region), but passes through a narrow unstable region according to some experimental results.

In case (2), the frequency parameter F = 230, which is the value corresponding to the critical point according to linear parallel-flow theory. Branch I of the neutral stability curve according to linear parallel-flow theory is located at x = 37.9 and the TS wavelength at that point is 4.5. Branch II is at x = 56.2, which is out of the domain considered here.

Instantaneous disturbance profiles vs. normal distance from the wall at every streamwise location x are given in Figure 15, after 5 cycles of forcing. After 5 cycles of forcing, when the majority of the flow (except at the region of the convecting disturbance wave front) has become time-periodic (quasi-steady), the amplitude (magnitude) of these periodic perturbations is determined from the last (5th) cycle. The amplitude vs. normal distance from the wall profiles are plotted in Figure 16.

The amplitude of the streamwise perturbation velocity obtained after subtracting the instantaneous Stokes-wave solution, at every streamwise location after x = 3.0 (the juncture of the flat plate and the ellipse) is shown in Figure 17. The amplitude profiles develop into TS wave amplitude profiles around x = 6.0. The receptivity, as defined by the ratio of TS wave amplitude to sound amplitude is of order 1, the maximum being 1.7 at x = 14.05. This trend of order 1 receptivity and the growth of disturbances outside the neutral curve of linear theory was also observed in the experiments (at a higher Reynolds number and lower frequency) by Shapiro (1977) and Leehey and Shapiro (1980). We attribute this to the pressure minimum and the subsequent small adverse pressure gradient near the leading edge. Due to the presence of this small adverse pressure gradient, the instability loop is expected to shift to the left and open up similar to stability diagrams for Falkner-Skan flows.

For F = 230 instantaneous disturbance profiles after 4 periods of forcing, and disturbance amplitude profiles (before the Stokes wave is subtracted) with respect to normal distance during the fourth cycle are given in Figures 18 and 19. After the Stokes wave is subtracted,disturbance profiles displayed in Figure 20 show clearly a transformation into TS wave profiles. The wavelength is 4.5 and the wavespeed is 0.395, which are about the same as the TS wavelength and wavespeed according to linear stability theory. The ratio of maximum amplitude of the TS wave to the sound-wave

amplitude is about 0.8, the maximum occurring at three grid points between x = 20.58 and x = 21.39. Compared to the high-frequency case (1), the amplitudes of the TS wave in this case are found to be smaller. We attribute this to the fact that the Branch I neutral point for a lower value of F is farther downstream (according to linear stability theory).

4.3 OBSERVATIONS

A numerical code has been developed to solve both steady and unsteady two-dimensional flow over a flat plate with an elliptic leading edge and finite thickness using the full incompressible Navier-Stokes equations in curvilinear coordinates. The present time-accurate code has allowed us to observe both the temporal and spatial initial development of the instability (TS) wave in the boundary layer due to imposed, freestream, long-wavelength disturbances. This is the first successful attempt to numerically simulate receptivity to freestream, time-harmonic oscillations on a realistic flat plate, offering possible explanations for discrepancies between experiments and various simplified numerical and theoretical models.

Some of the important conclusions that can be inferred thus far are:

i) The experimental results of early growth of TS waves before the Branch I neutral-stability point and order 1 receptivity are observed, and can be attributed to the adverse pressure gradient existing near the blunt leading edge.

ii) The observance of TS wave growth with F = 333 is in accordance with some experimental observations and indicates that the discrepancies in neutral stability curves between linear stability theory and experiments at high frequencies can be due to small mean adverse pressure gradients existing near the leading edge.

iii) The receptivity mechanism to freestream, time-harmonic, long-wavelength oscillations, which has been observed in experiments is verified to some extent in this study and can be described as follows:

A long-wavelength, streamwise velocity perturbation, which closely simulates a plane sound wave travelling parallel to the plate in an incompressible limit, has to diffract at the leading edge, which introduces spatial variations in fluctuations of both u' and v' components at the leading edge (near the stagnation point), or, in other words, introduces unsteady fluctuations in pressure that vary with tangential direction along the wall. This, in turn, generates fluctuating vorticity at the leading edge, the majority of which is convected downstream in the boundary layer. This convected vorticity wave soon matches or develops into instability waves (TS waves) of the laminar boundary layer.

iv) Up to the periods of calculations presented here, interaction between the TS wave and the travelling sound wave occurs only at the leading edge region.

v) Some qualitative features predicted by the theory of Goldstein (1983) are observed, although the orders of receptivity differ. The quantitative measure of receptivity here, i.e. the ratio of amplitude of the TS wave to that of the freestream disturbance, definitely depends on the leading-edge radius of curvature, and hence the pressure gradient there.

This work is being extended to three-dimensional basic states and disturbance fields as described in Section 3.

## 5. RESOURCES AND PERSONNEL

One of the principal strengths of our team at Arizona State University is its broad skills in analysis, computations, and experiments. We facilitate day-to-day communication between the computational work and the experimental work through an IRIS 3030 Graphics Workstation. The system, with state-of-the-art, real-time, three-dimensional, color-graphics software (PLOT3D), is equipped with an extensive multi-user and multi-task environment with twelve serial lines. Users are able to share the same data base or experimental information. This provides the heart of the interaction of the analytical, computational, and experimental research.

In addition to the super computers at NASA facilities and Princeton/NSF Consortium, the network includes access to the IBM 4341/VM and Harris/VS computers, the IBM 3090 Class VI machine, and the Cray on campus as well as the MASSCOMP. The College of Engineering at ASU is currently also equipped with several VAX/780 and VAX/785 minicomputers exclusively for research purposes (each office and laboratory has a hard-wired RS232 interface). These minicomputers are excellent systems for program development. The IRIS can access all the features available in those minicomputers through the existing local area networking (Ethernet) on the campus. Furthermore, the system can communicate directly with NASA research facilities to share information through telephone couplings. The full array of computer capabilities from super-mini to super-super was in place for the research.

The principal investigator for this work is Helen L. Reed, Associate Professor of Mechanical and Aerospace Engineering. Professor Reed has spent the last nine years conducting theoretical and computational research on problems of boundary-layer stability specifically applied to the ACEE/LFC programs.

## 6. REFERENCES

Collier, F.S. Jr. and Malik, M.R. 1989. "Curvature effects on the stability of three-dimensional laminar boundary layers," AGARD-CP-438, Fluid Dynamics of Three-Dimensional Turbulent Shear Flows and Transition, Cesme, Turkey, 3-6 October, No. 10.

Collier, F.S. Jr. et al. 1989. Presentation at ICASE Workshop on Instability and Transition in Session on Crossflow Instability, May-June.

Fasel, H. 1980. Recent developments in the numerical solution of the Navier-Stokes equations and hydrodynamic stability problems. Comp. Fluid Dyn., Kollman and Wolfgang eds., Hemisphere.

Gedney, C.J. 1983. The cancellation of a sound-excited Tollmien-Schlichting wave with plate vibration. Phys. Fluids 26, 5, 1158-1160.

Goldstein, M.E. 1983a. The evolution of Tollmien-Schlichting waves near a leading edge. J. Fluid Mech. 127, 59.

Goldstein, M.E., Sockol, P.M. and Sanz, J. 1983b. The evolution of Tollmien-Schlichting waves near a leading edge. Part 2. Numerical determination of amplitudes. J. Fluid Mech. 129, 443.

Goldstein, M.E. and Hultgren, L.S. 1989. Boundary-layer receptivity to long-wave free-stream disturbances. Ann. Rev. Fluid Mech. 21, 137-66.

Herbert, Th. 1985. Three-dimensional phenomena in the transitional flat-plate boundary layer. AIAA-85-0489.

Hussaini, M.Y. and Zang, T.A. 1987. "Spectral methods in fluid dynamics," Annual Review of Fluid Mechanics.

Kleiser, L. and Schumann, U. 1984. "Spectral simulations of the laminar-turbulent transition process in plane Poiseuille flow," Spectral Methods for Partial Differential Equations, ed. R. Voigt, D. Gottlieb, and M. Hussaini, SIAM.

Leehey, P. and Shapiro, P.J. 1980. Leading edge effect in laminar boundary layer excitation by sound. Laminar-Turbulent Transition, Springer-Verlag, 321-331.

Mack, L.M. 1977. Transition prediction and linear stability theory. AGARD C-P No. 224, 1.

Morkovin, M.V. 1978. Instability, transition to turbulence and predictability. AGARDograph No. 236.

Morkovin, M.V. 1983. Understanding transition to turbulence in shear layers - 1983. AFOSR Final Report, Contract F49620-77-C-0013.

Orszag, S.A. and Kells, L.C. 1980. Transition to turbulence in plane Poiseuille and plane Couette flow. J. Fluid Mech. 96.

Reshotko, E. 1984. Environment and receptivity. AGARD Report No. 709 (Special course on stability and transition of laminar flows) VKI, Brussels, March 1984.

Saric, W.S. 1985a. Stability and transition in bounded shear flows. Proc. Persp. Fluid Mech., Caltech, Jan. 1985.

Saric, W.S. 1985b. Boundary-layer transition: T-S waves and crossflow mechanisms. Proc. AGARD Special Course on Aircraft Drag Prediction and Reduction, VKI, Belgium, May 1985.

Saric, W.S. 1985c. Laminar flow control with suction: theory and experiment. Proc. AGARD Special Course on Aircraft Drag Prediction and Reduction, VKI, Belgium, May 1985.

Shapiro, P.J. 1977. The influence of sound upon laminar boundary layer instability. MIT Acoustics & Vibration Lab. rep. 83458-83560-1.

Singer, B.A., Reed, H.L. and Ferziger, J.H. 1989. The effect of streamwise vortices on transition in the plane channel. Accepted Phys. Fluids.

Tani, I. 1980. Three-dimensional aspects of boundary-layer transition. Reprint: Visiting Scholar Lectures, VPI & SU, Oct. 1980.

# 7. FIGURES

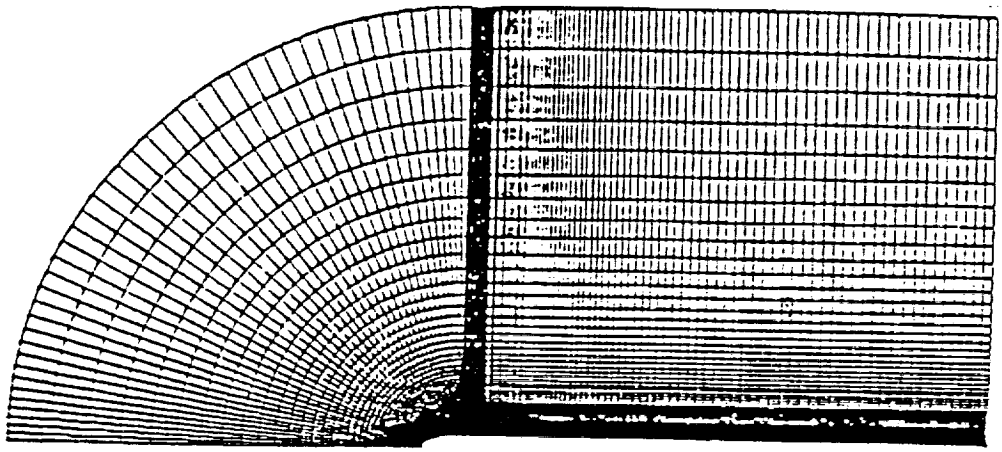

a. Generated C-grid

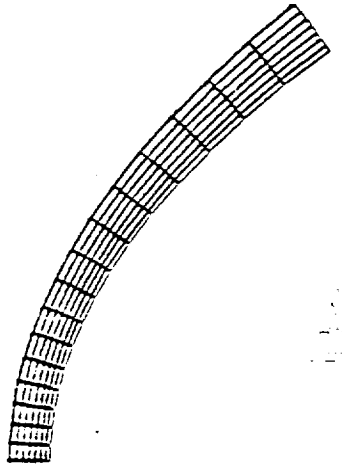

b. Enlarged view at the leading edge

Figure 1. Generated grid over the semi-infinite flat plate; AR=3.

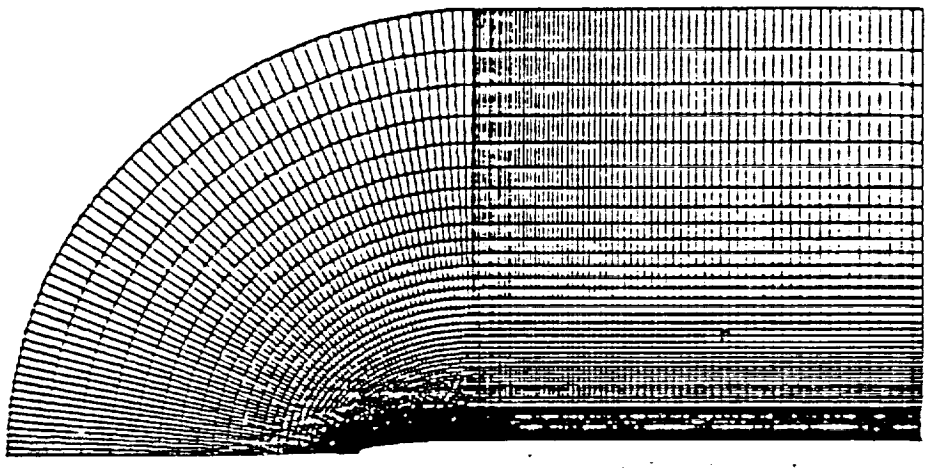

a. Generated C-grid

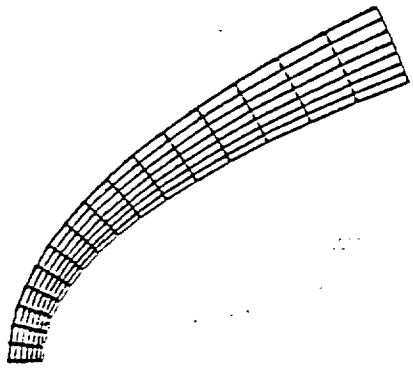

b. Enlarged view at the leading edge

Figure 2. Generated grid over the semi-infinite flat plate; AR=9.

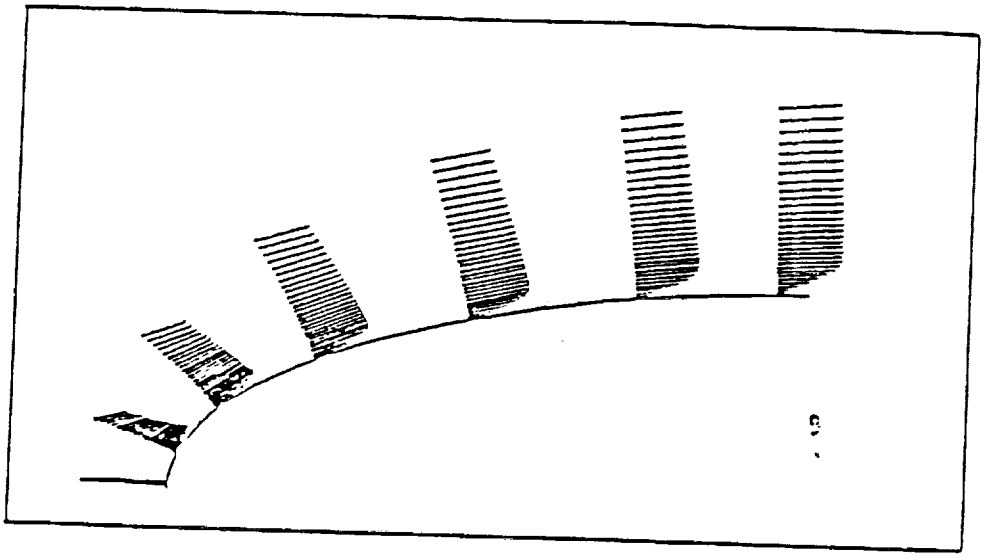

a. Leading edge region.

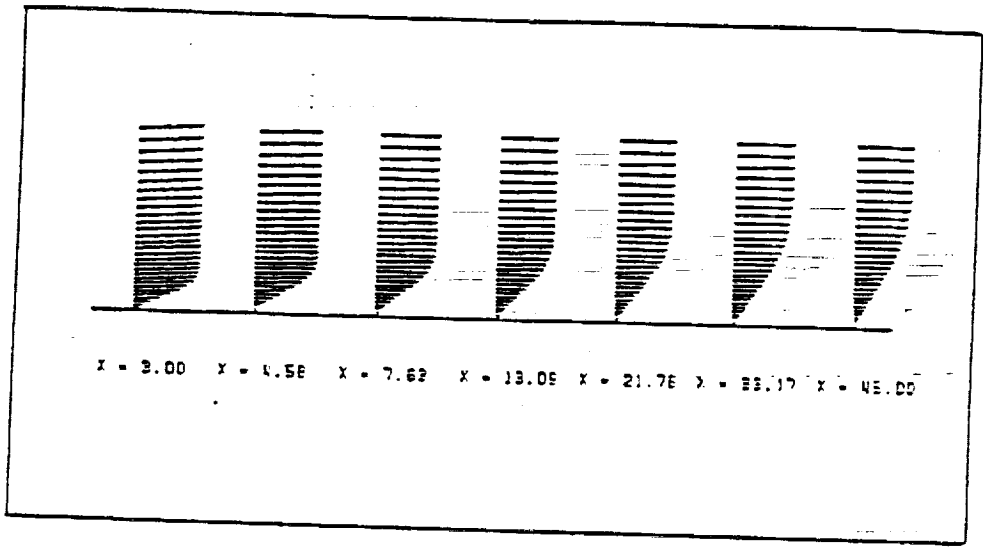


b. Flat plate region.

Figure 3. Steady state velocity vector profiles ; AR = 3, $Re_L$ = 2400.

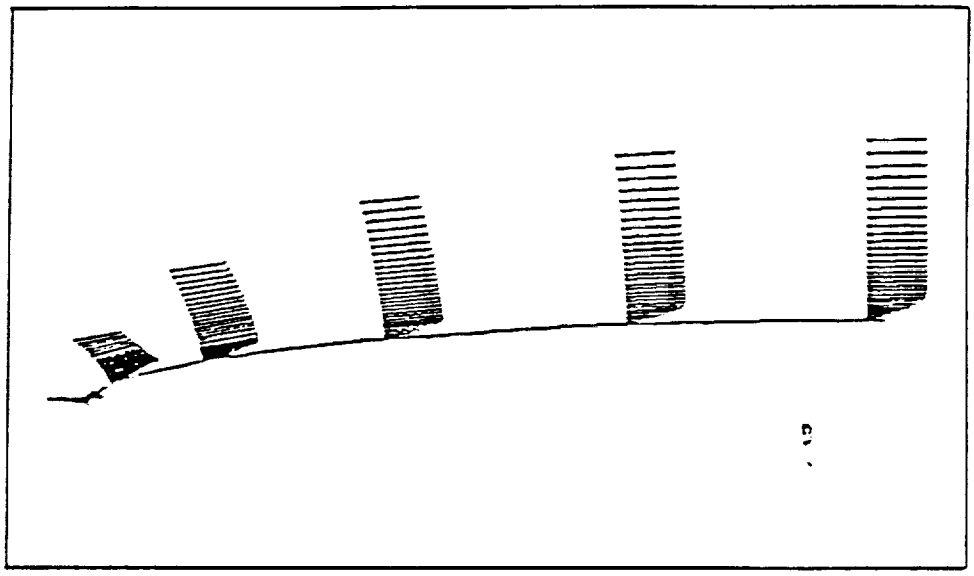

a. Leading edge region.

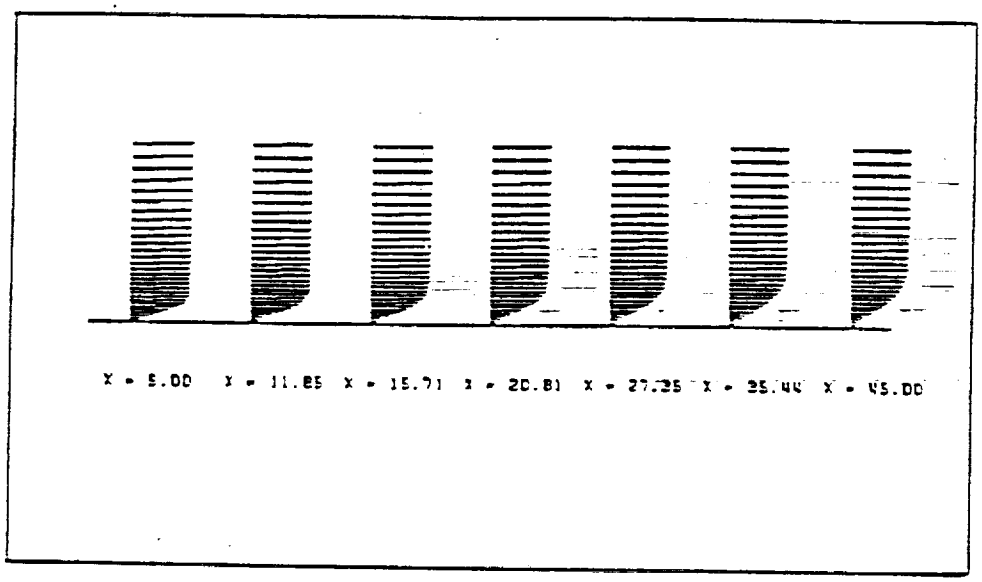


b. Flat plate region.

Figure 4. Steady state velocity vector profiles ; AR = 9, $Re_L$ = 2400.

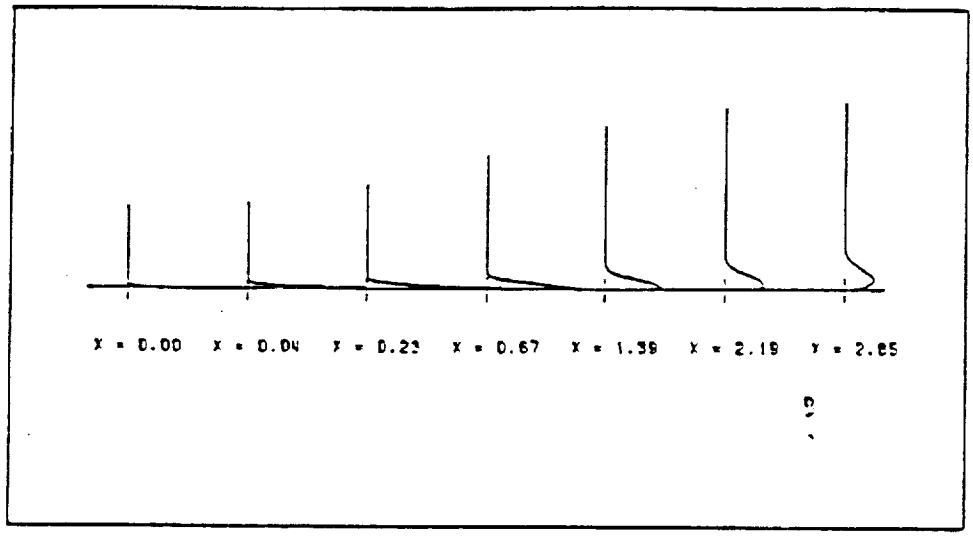


a. Leading edge region.

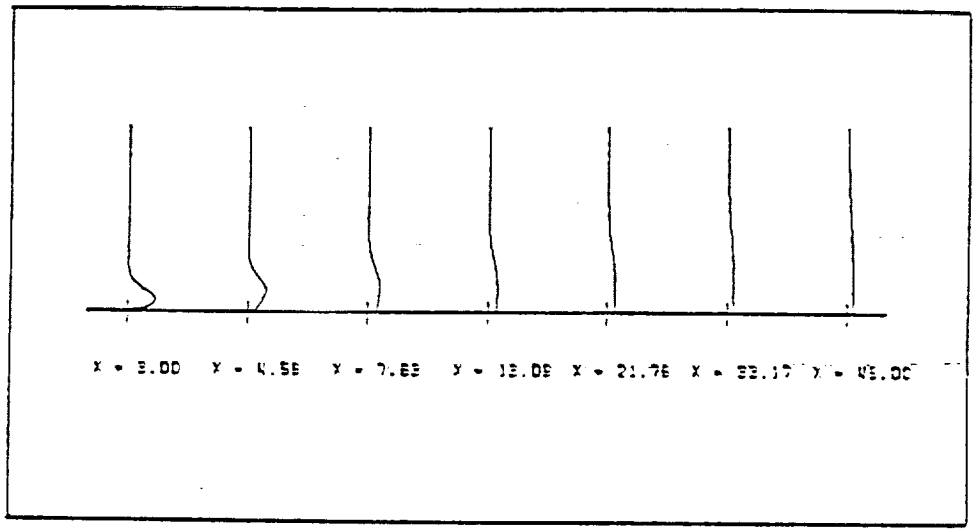


b. Flat plate region.

Figure 5. Steady state vorticity profiles vs. normal distance; AR = 3, $Re_L$ = 2400.

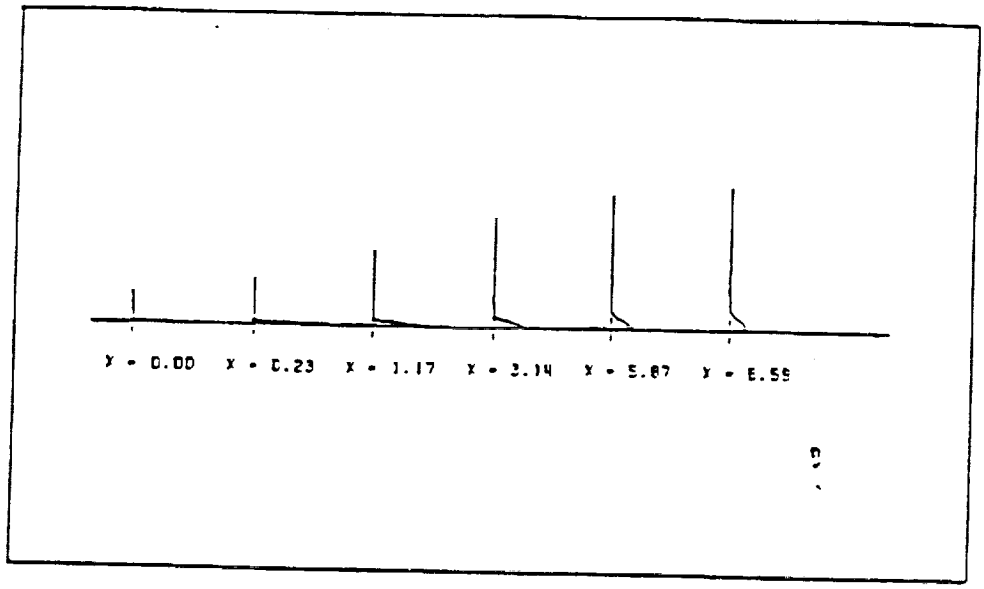


a. Leading edge region.

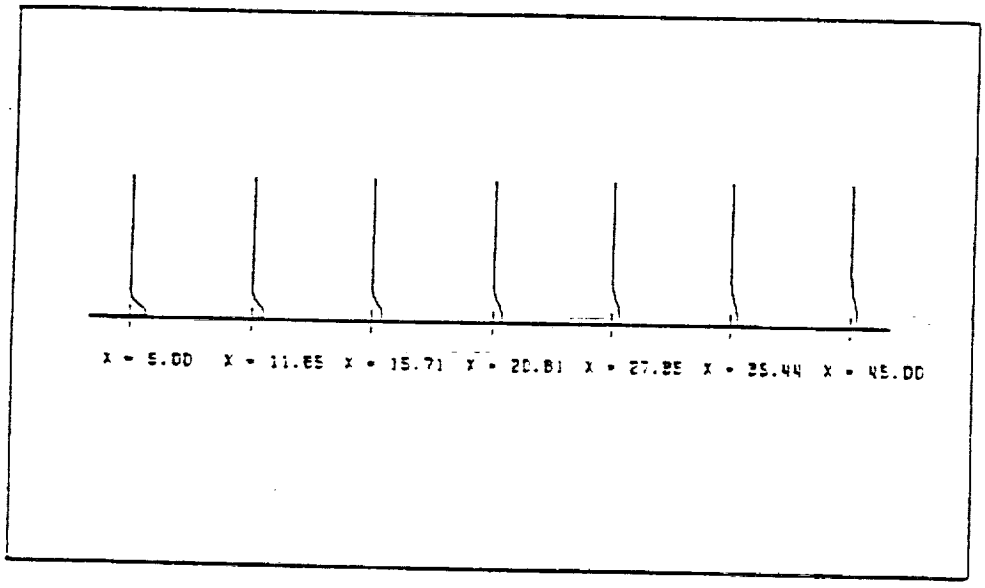


b. Flat plate region.

Figure 6. Steady state vorticity profiles vs. normal distance; AR = 9, $Re_L$ = 2400.

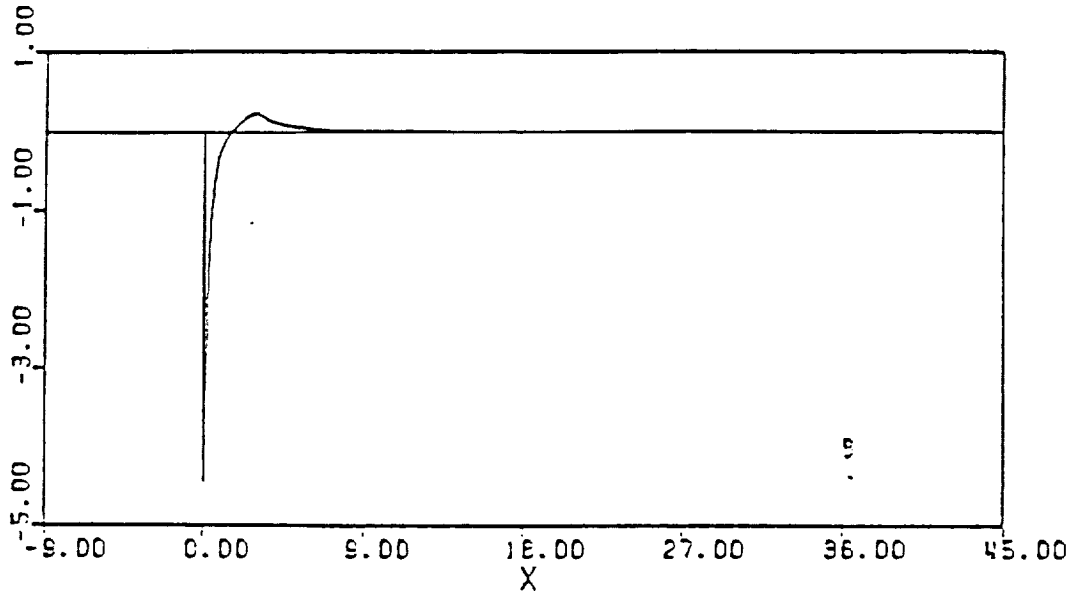


Figure 7. Pressure gradient along the wall; AR = 3, $Re_L$ = 2400.

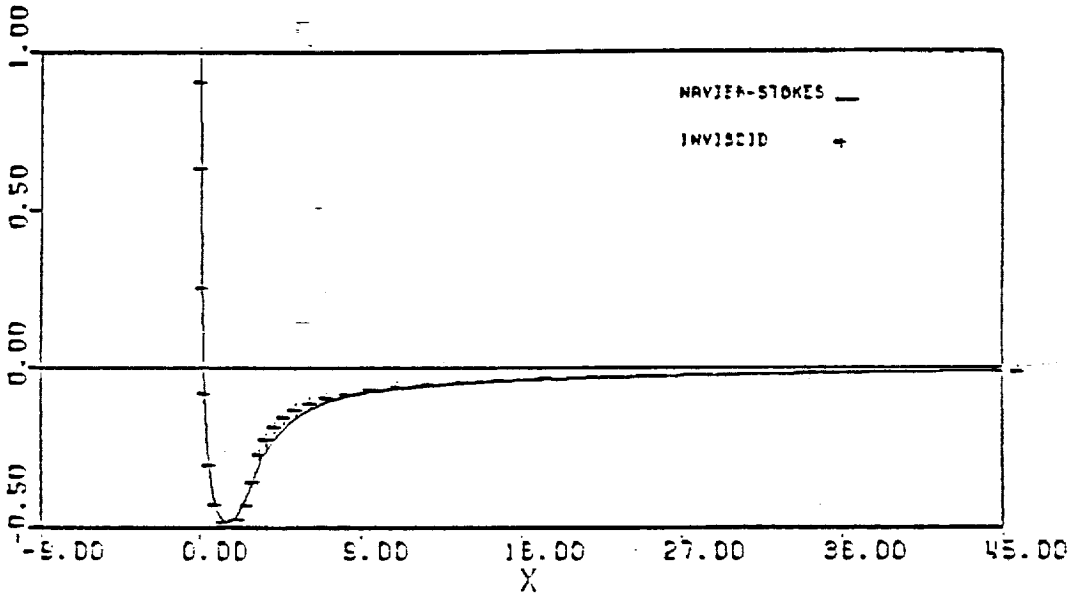


Figure 8. Surface pressure coefficient $C_p$; AR = 3; $Re_L$ = 2400.

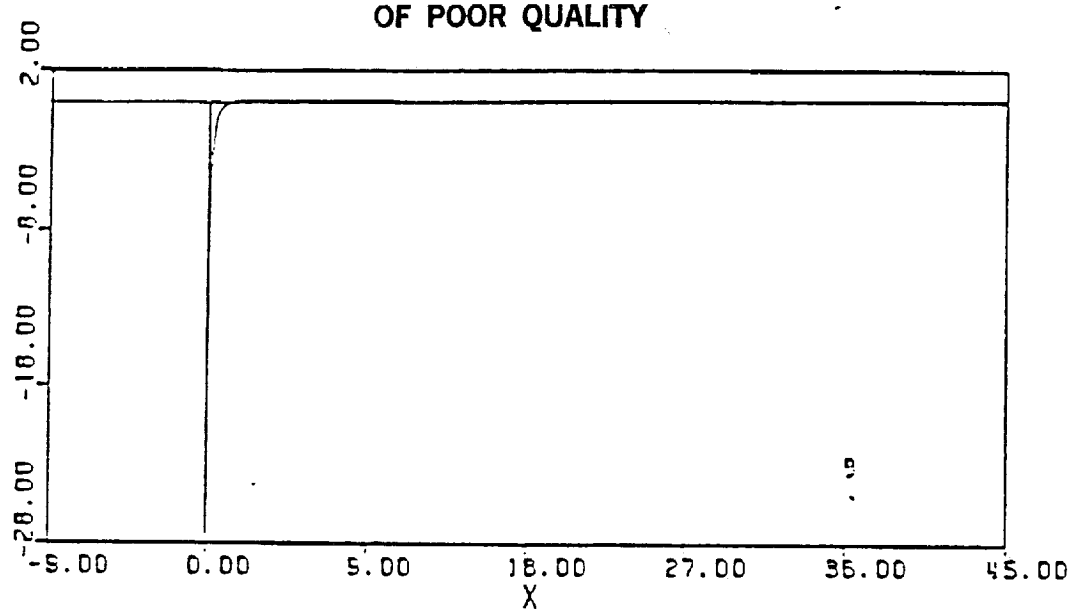


Figure 9. Pressure gradient along the wall; AR = 9, $Re_L$ = 2400.

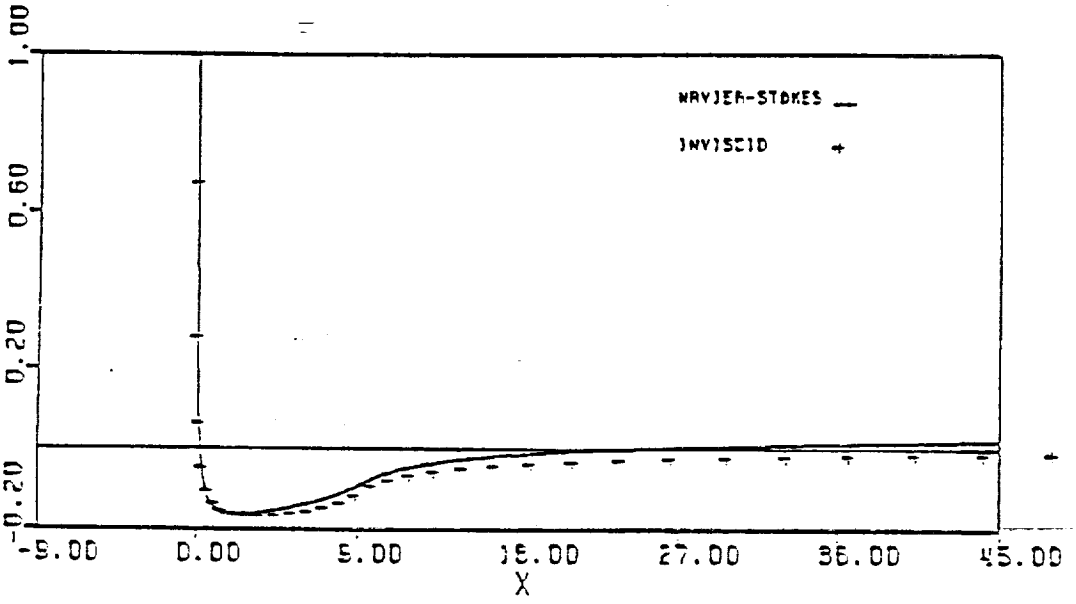


Figure 10. Surface pressure coefficient $C_p$; AR = 9, $Re_L$ = 2400.

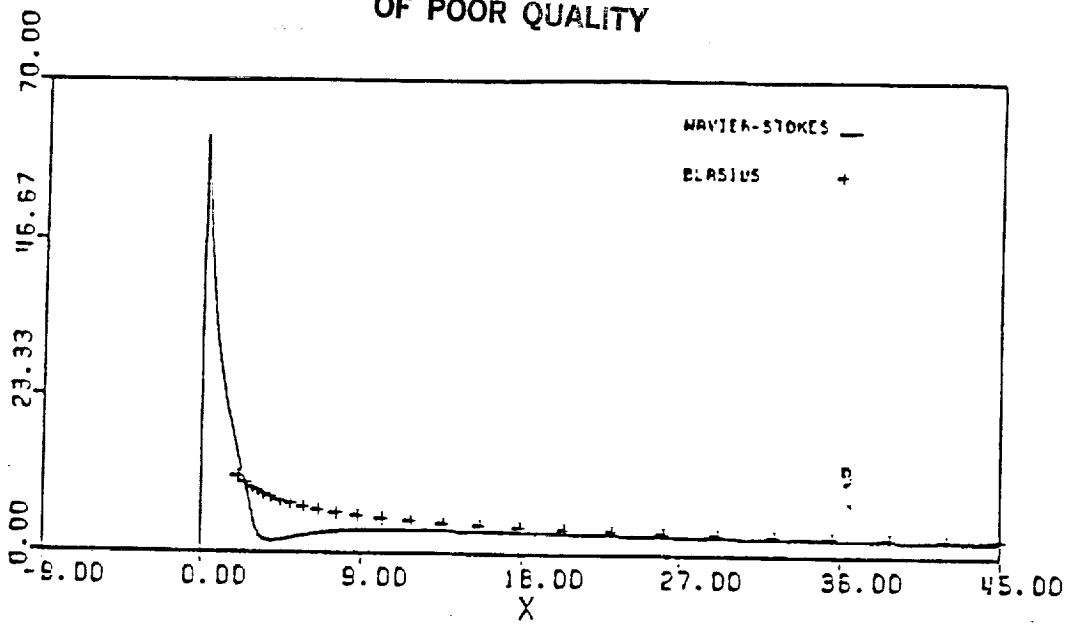


Figure 11. Wall vorticity distribution; AR = 3, $Re_L$ = 2400.

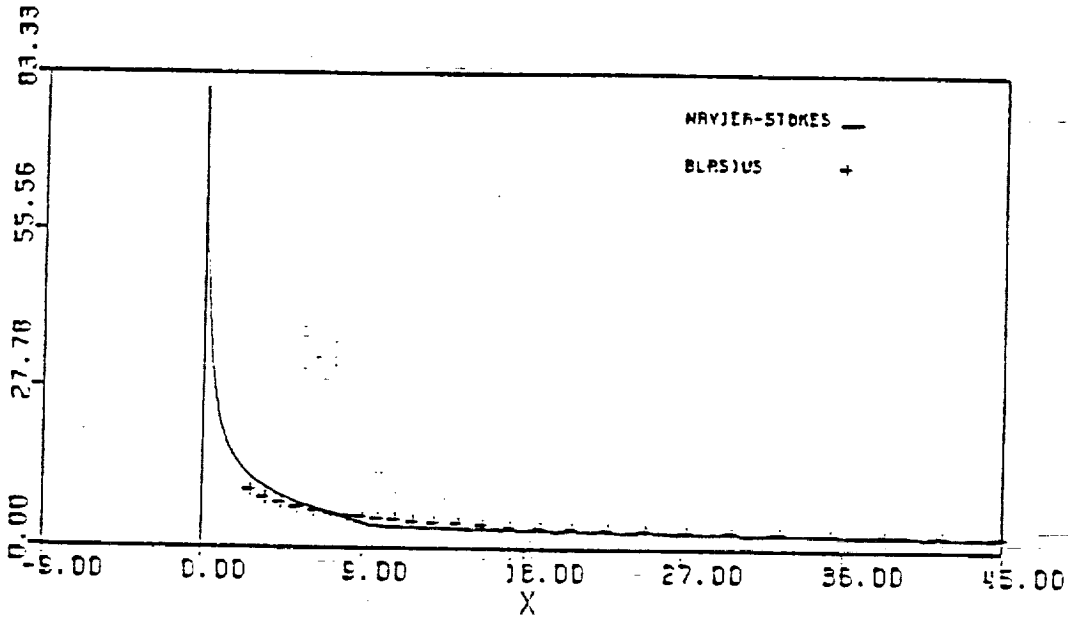


Figure 12. Wall vorticity distribution; AR = 9, $Re_L$ = 2400.

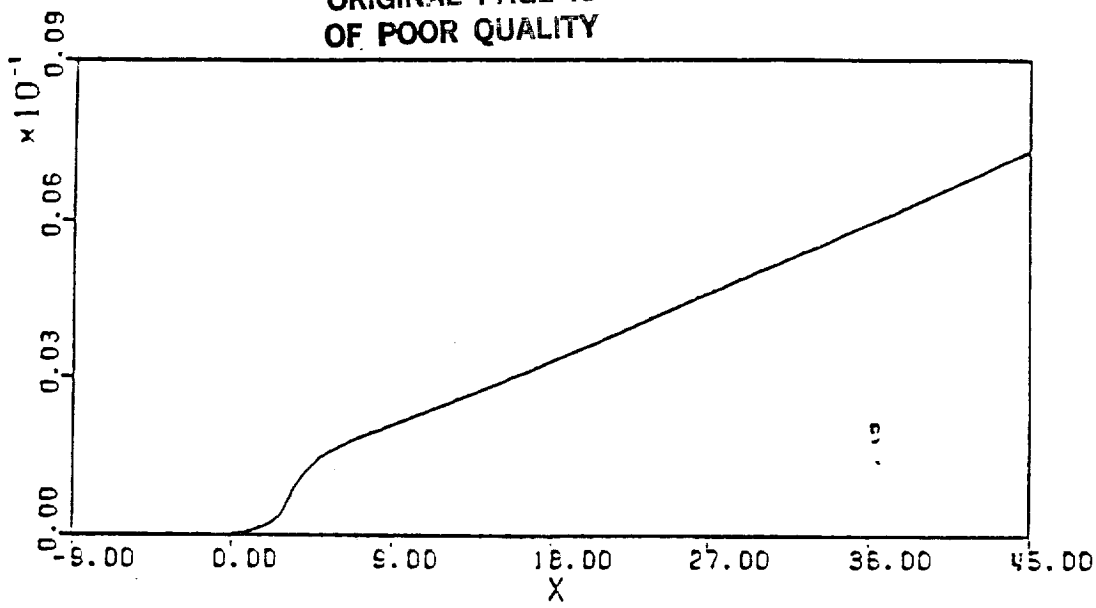


Figure 13. Square of the displacement thickness $\delta^{*2}$ vs. x; AR=3, $Re_L$ = 2400.

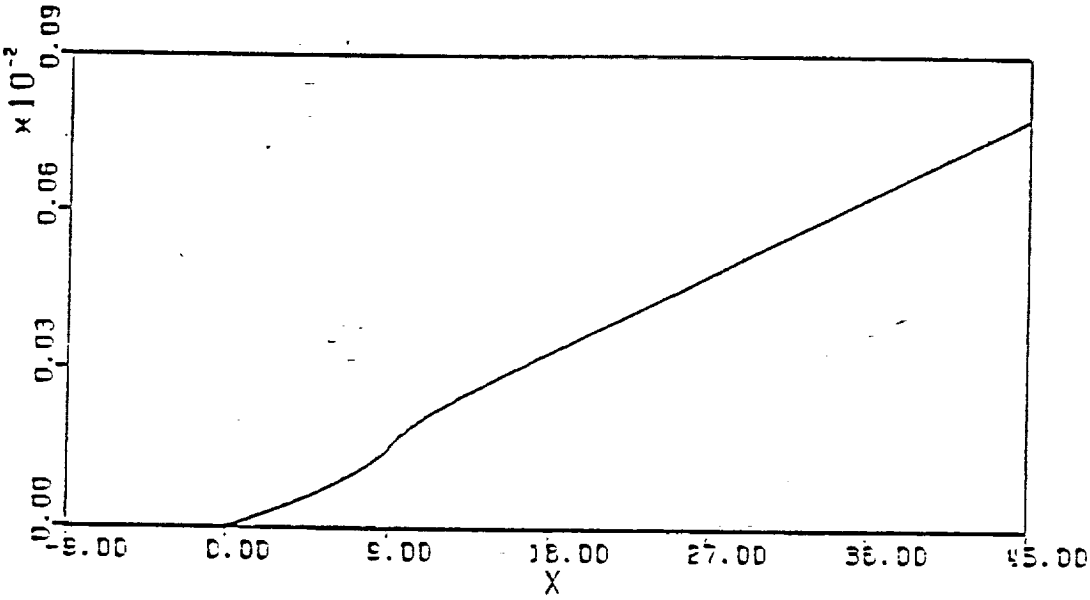


Figure 14. Square of the displacement thickness $\delta^{*2}$ vs. x; AR = 9, $Re_L$ = 2400.

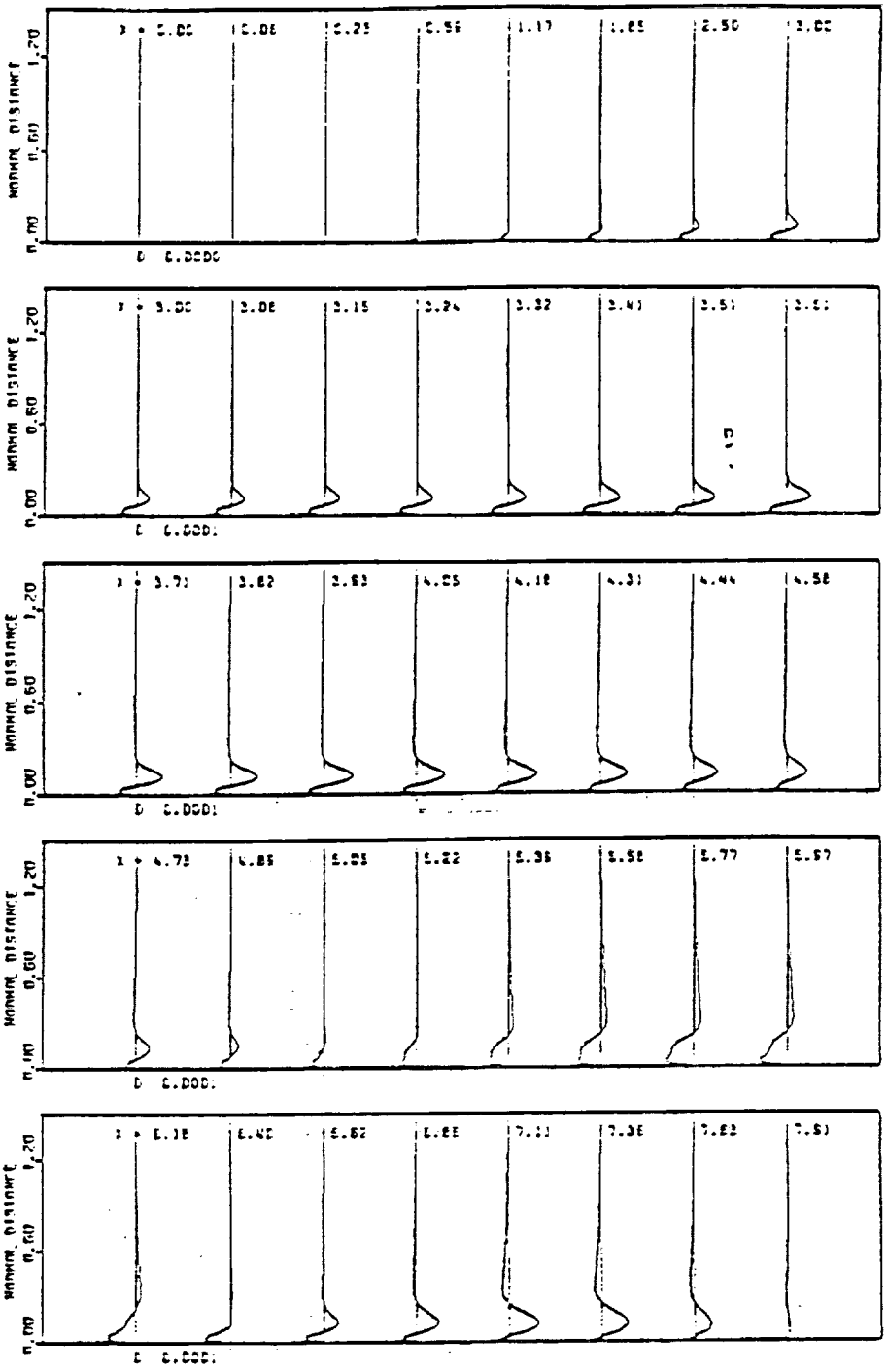

a. streamwise perturbation velocity, u'

Figure 15. Instantaneous perturbation profiles at consecutive... downstream locations after five periods of forcing; $F = 325$, $a_s = 0.0001$. ...

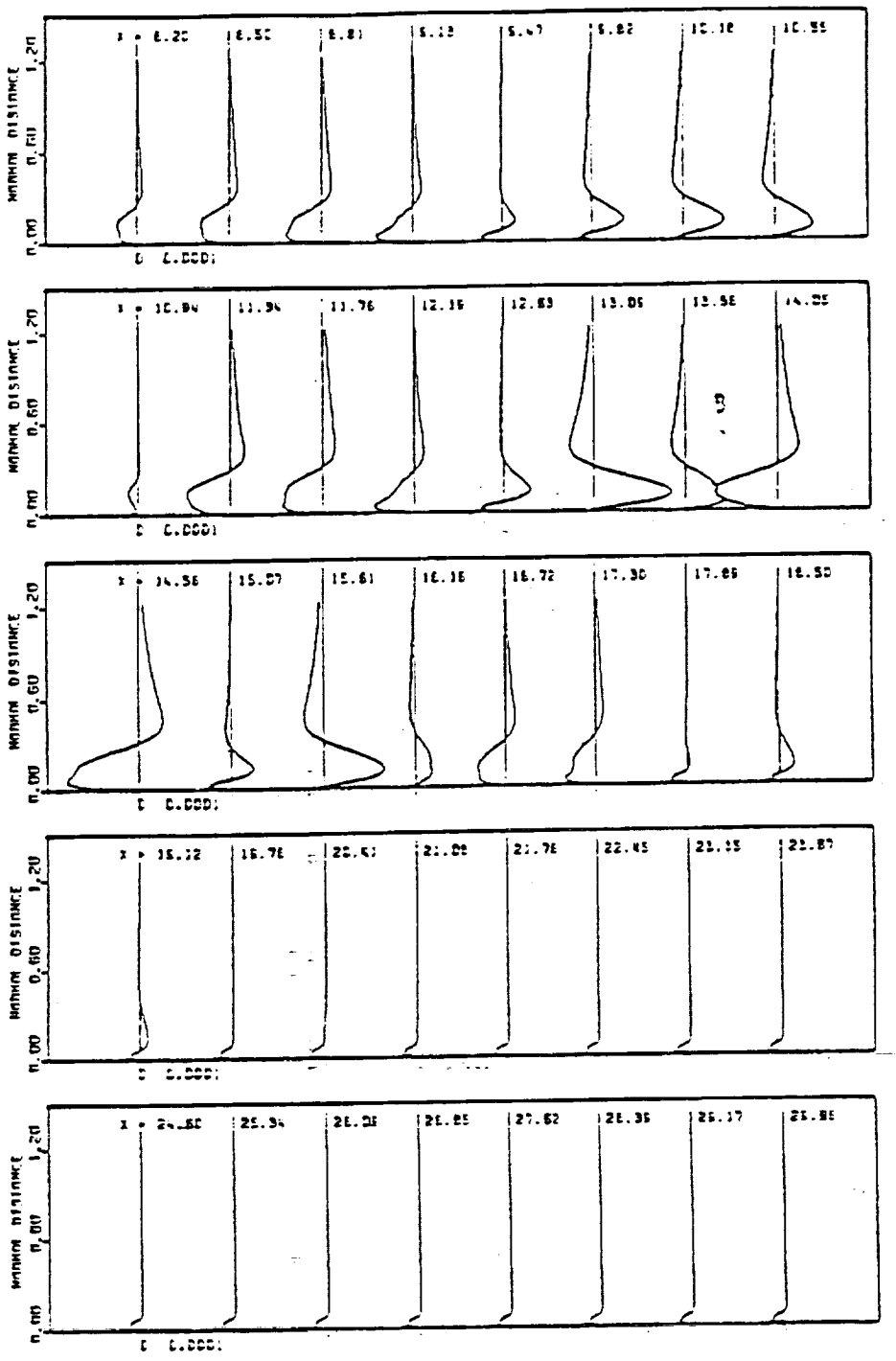


Figure 15a. Continued.

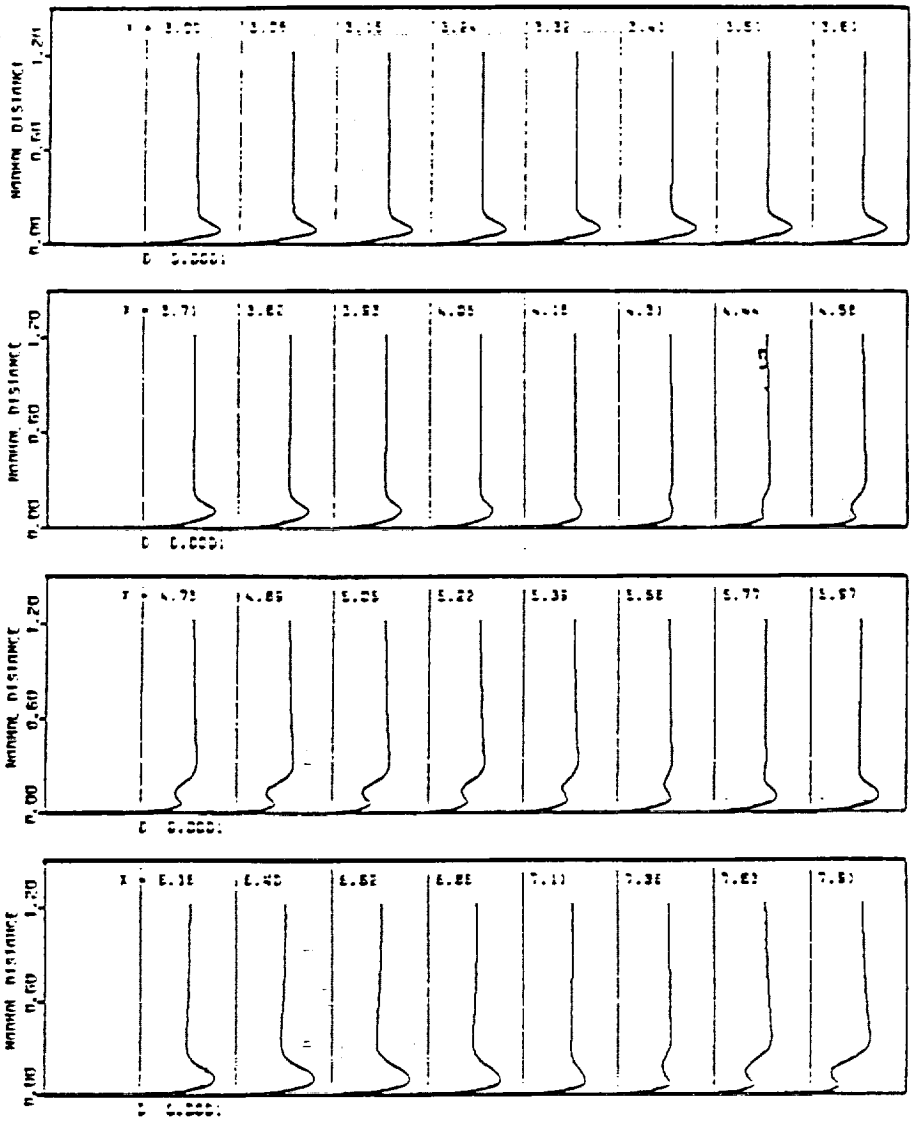

a. streamwise perturbation velocity, u'

Figure 16. Perturbation amplitude profiles taken during the fifth cycle at consecutive downstream locations before the Stokes wave is subtracted; $F = 325$, $a_s = 0.0001$.

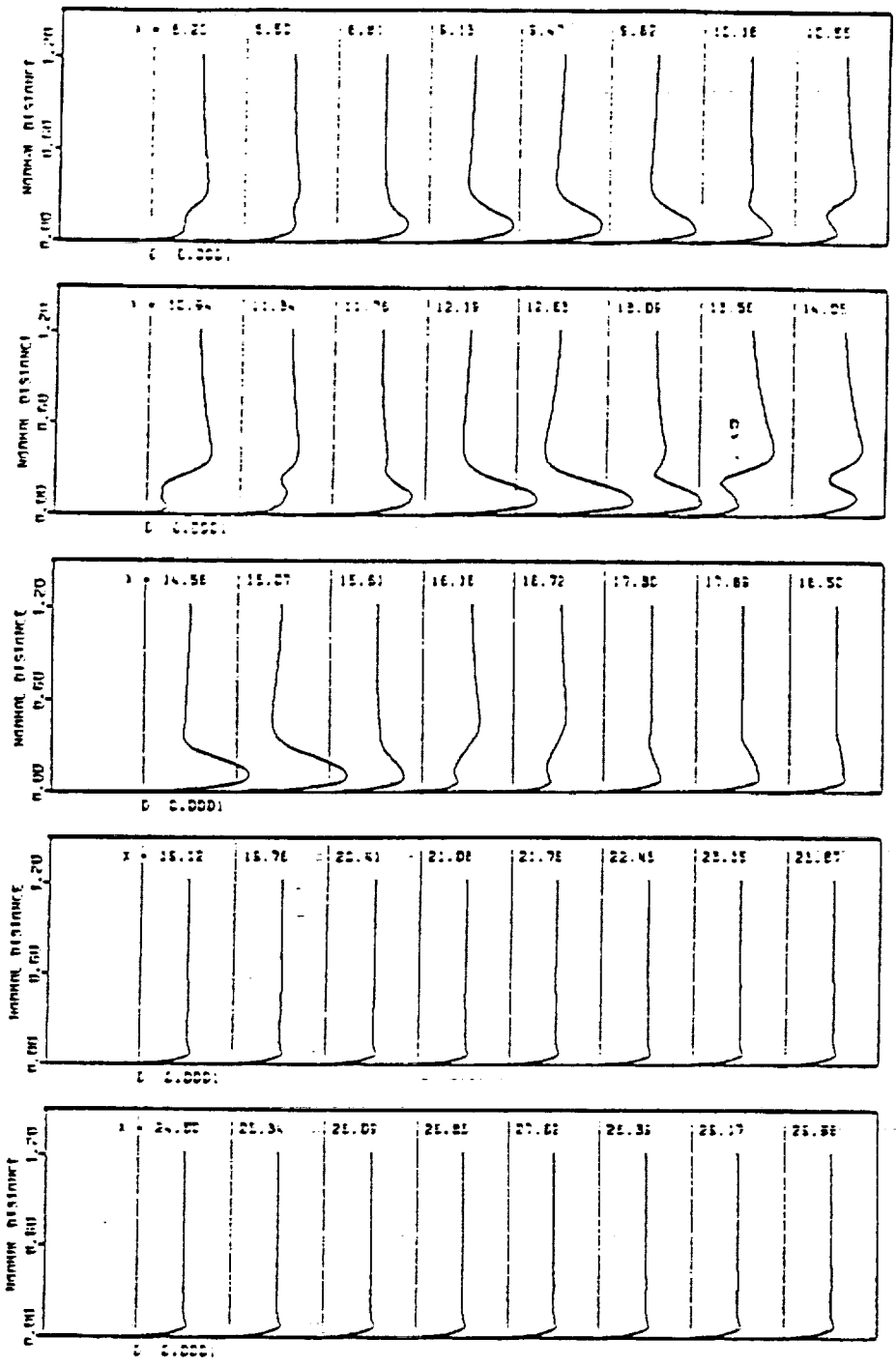

Figure 16a. Continued.

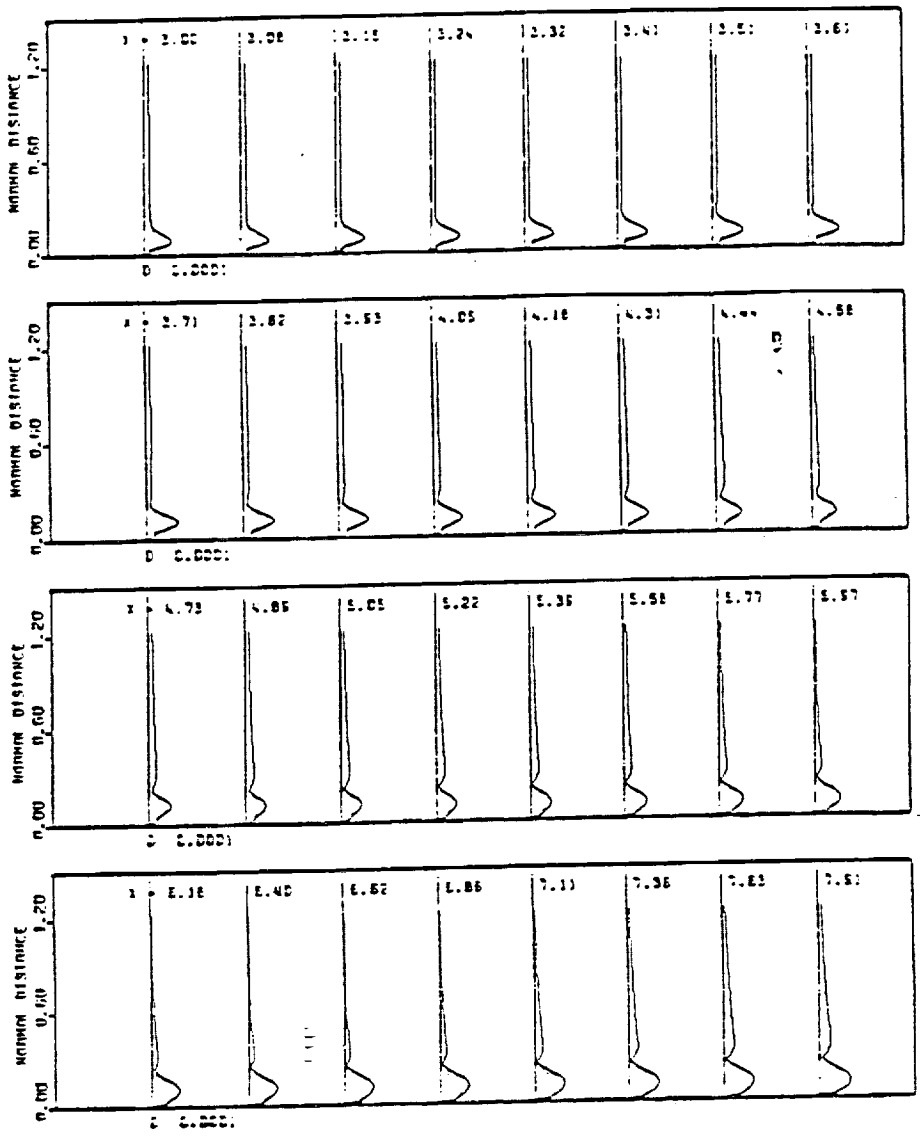

Figure 17. Amplitude profiles of streamwise perturbation velocity u' taken during the fifth cycle at consecutive downstream locations after the Stokes wave is subtracted; F = 325, $a_s$= 0.0001.

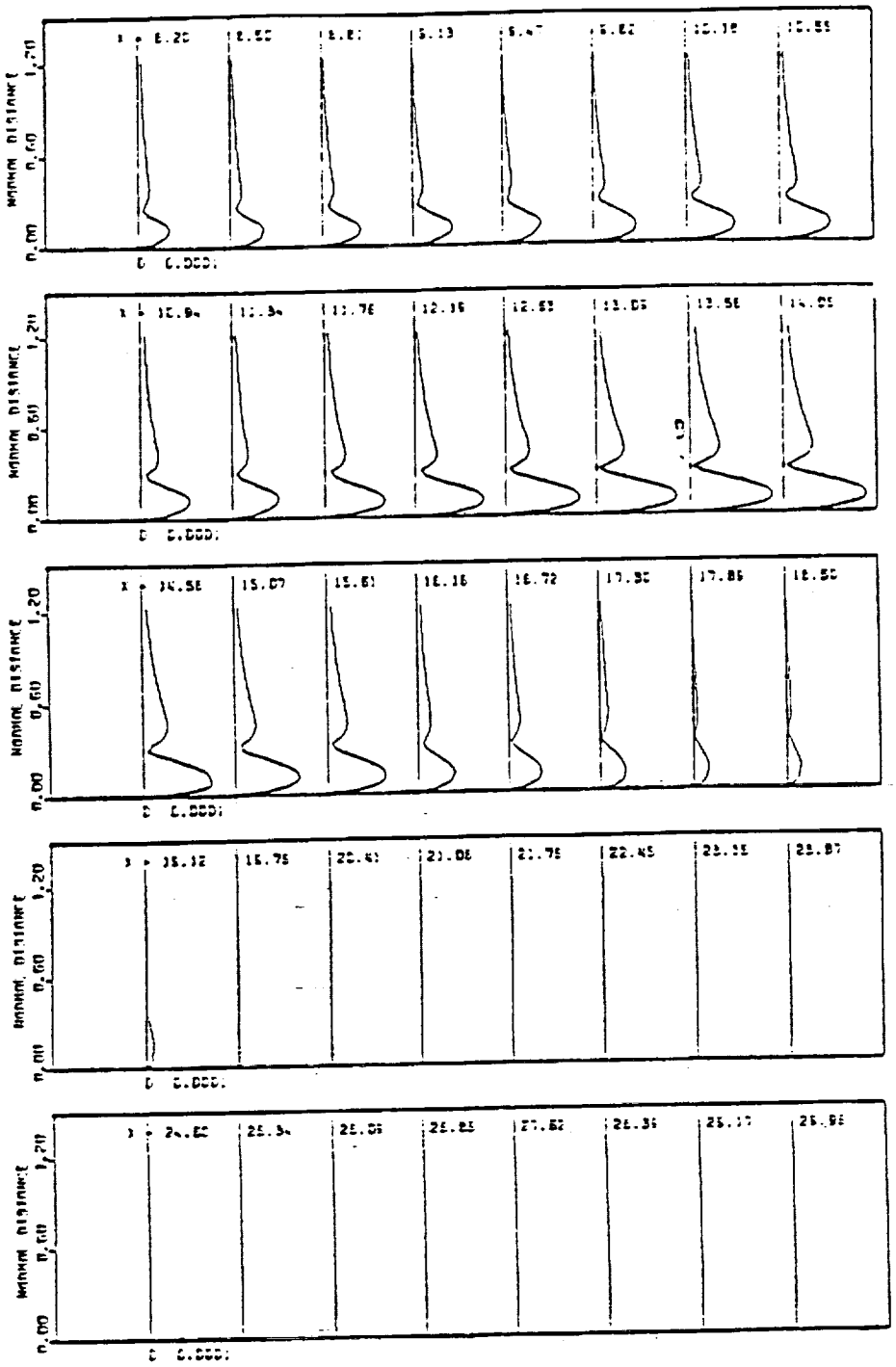

Figure 17a. Continued.

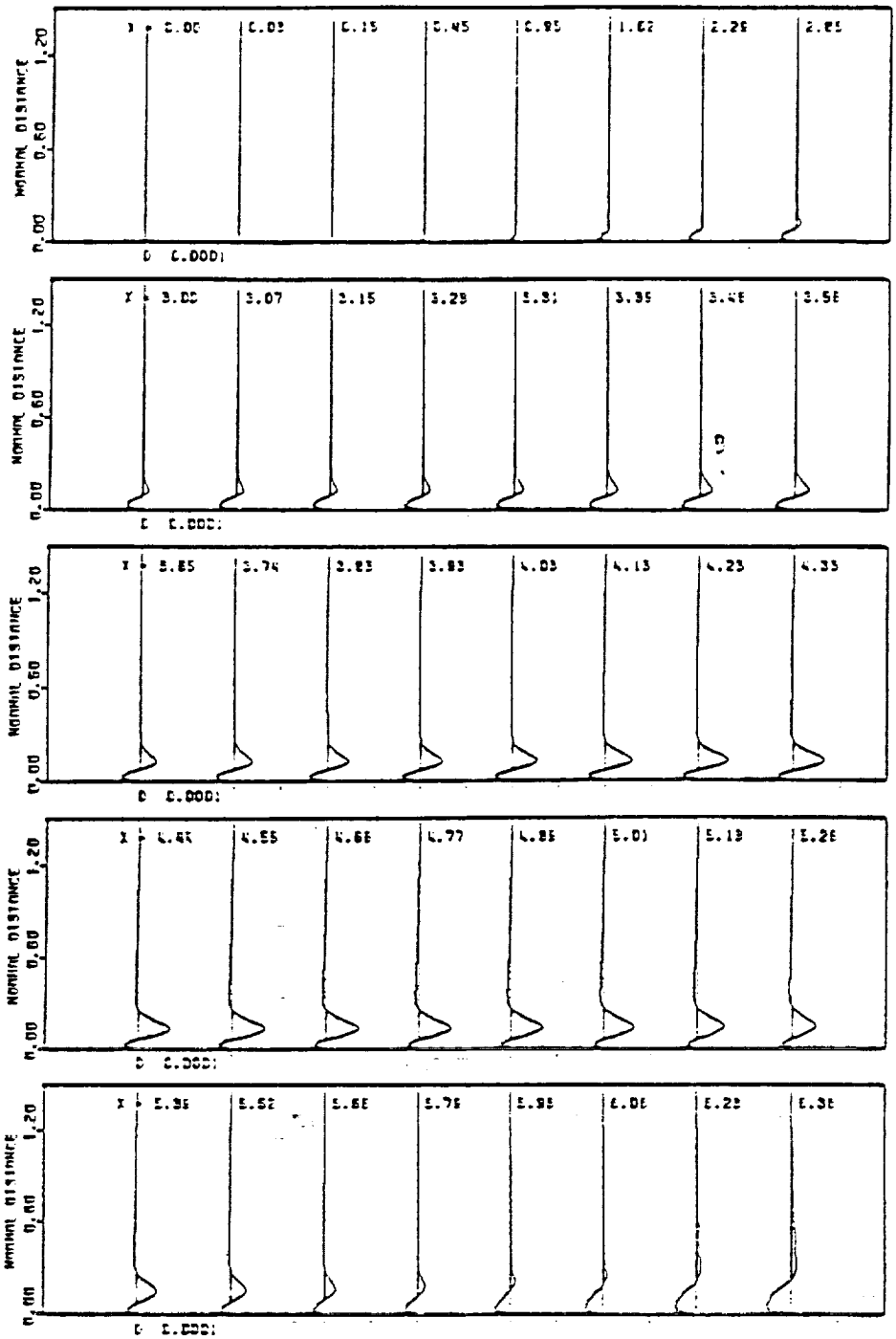

a. streamwise perturbation velocity, u'

Figure 18. Instantaneous perturbation profiles at consecutive downstream locations after four periods of forcing; F = 230, $\varepsilon_s$ = 0.0001.

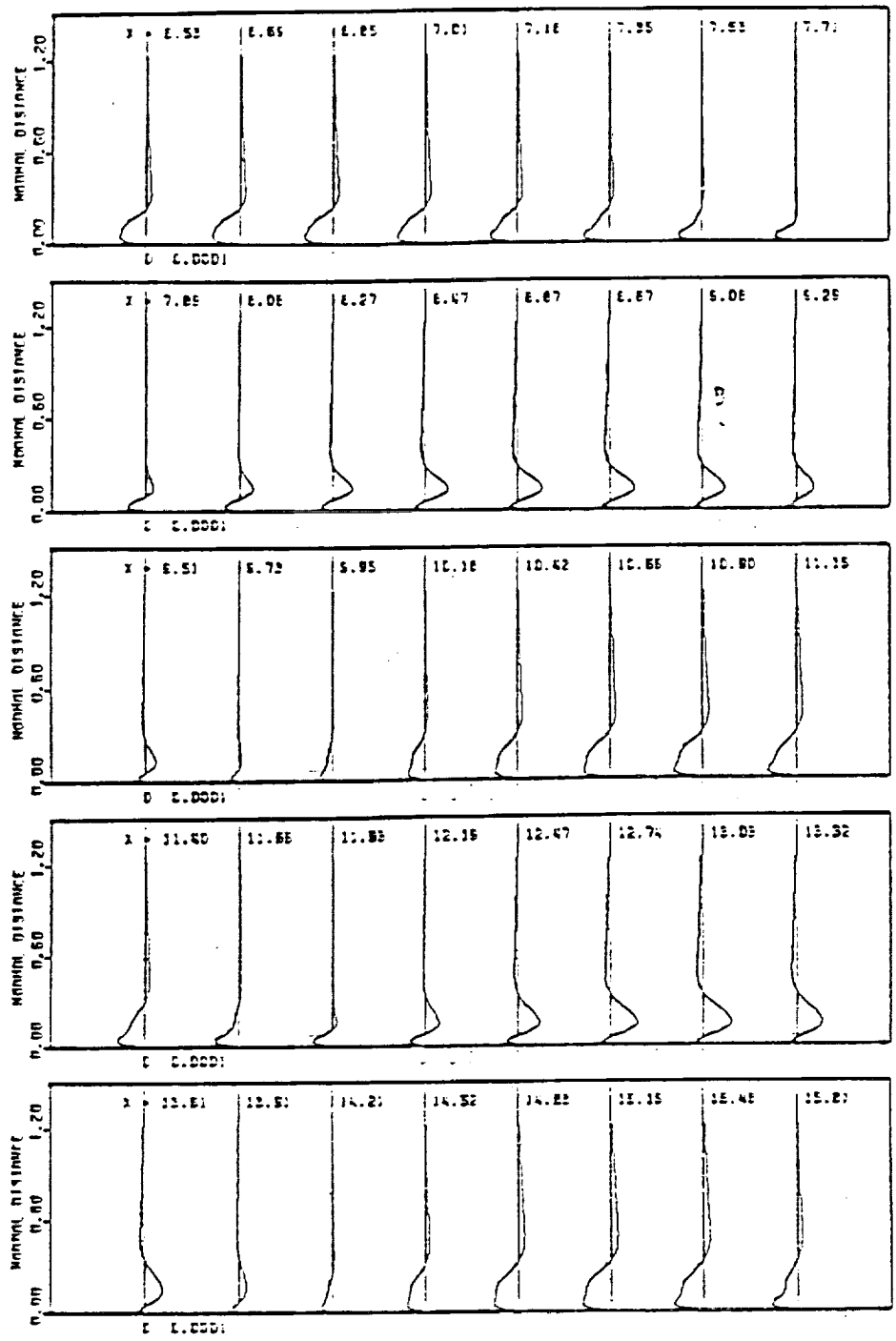


Figure 18a. Continued.

ORIGINAL PAGE IS
OF POOR QUALITY

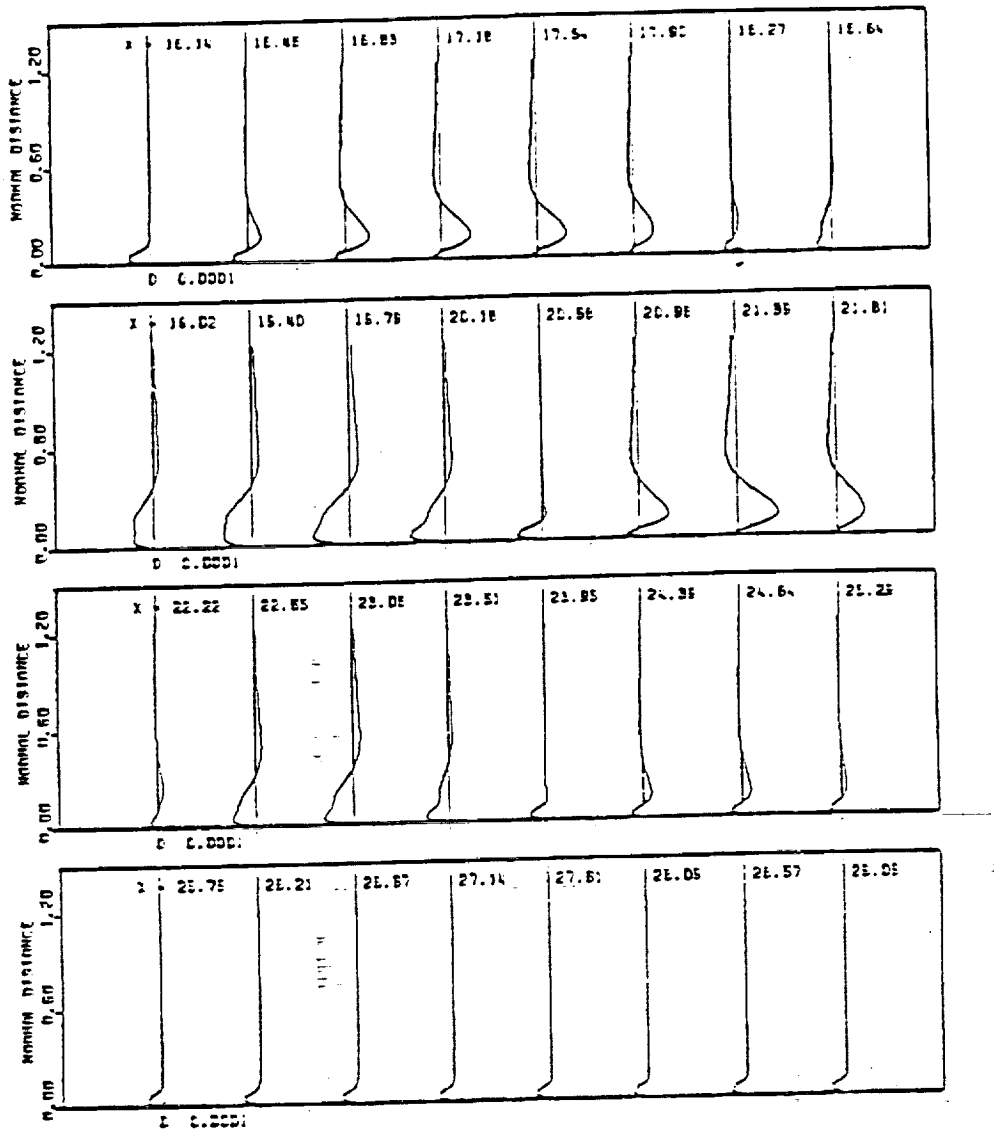


Figure 18a. Continued.

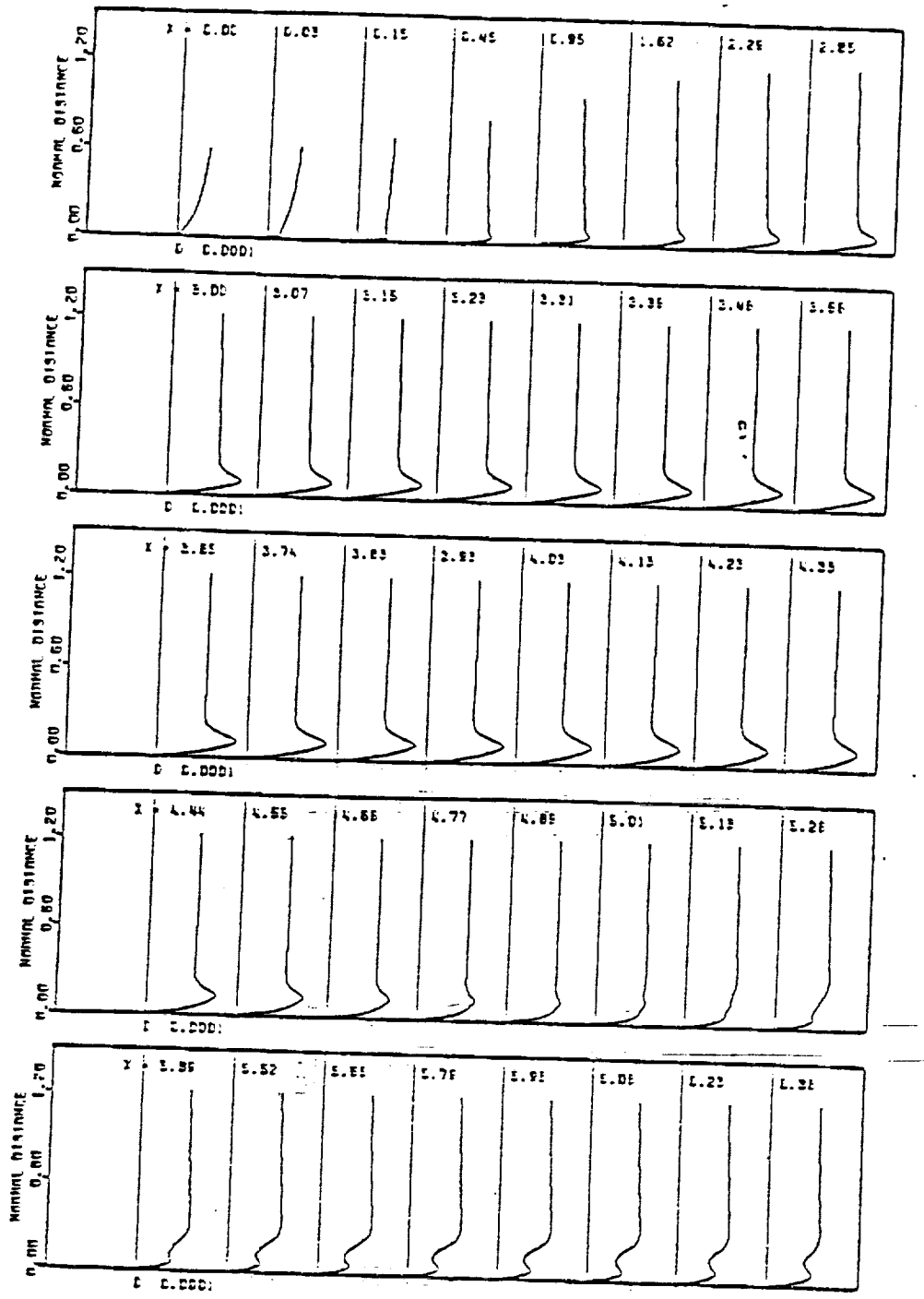

a. streamwise perturbation velocity, u'

Figure 19. Perturbation amplitude profiles taken during the fourth cycle at consecutive downstream locations before the Stokes wave is subtracted; $F = 230$, $a_s = 0.0001$.

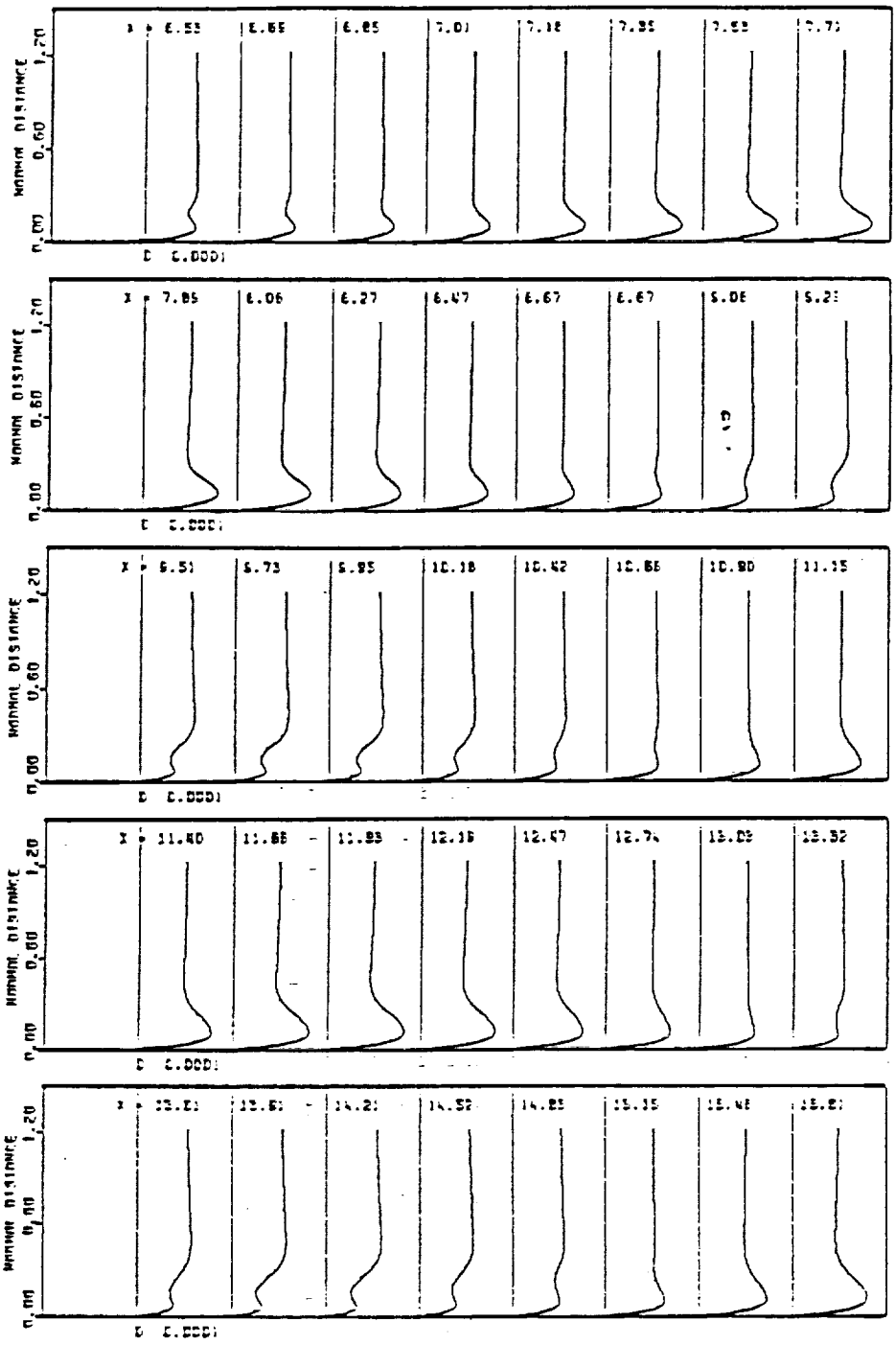

Figure 19a. Continued.

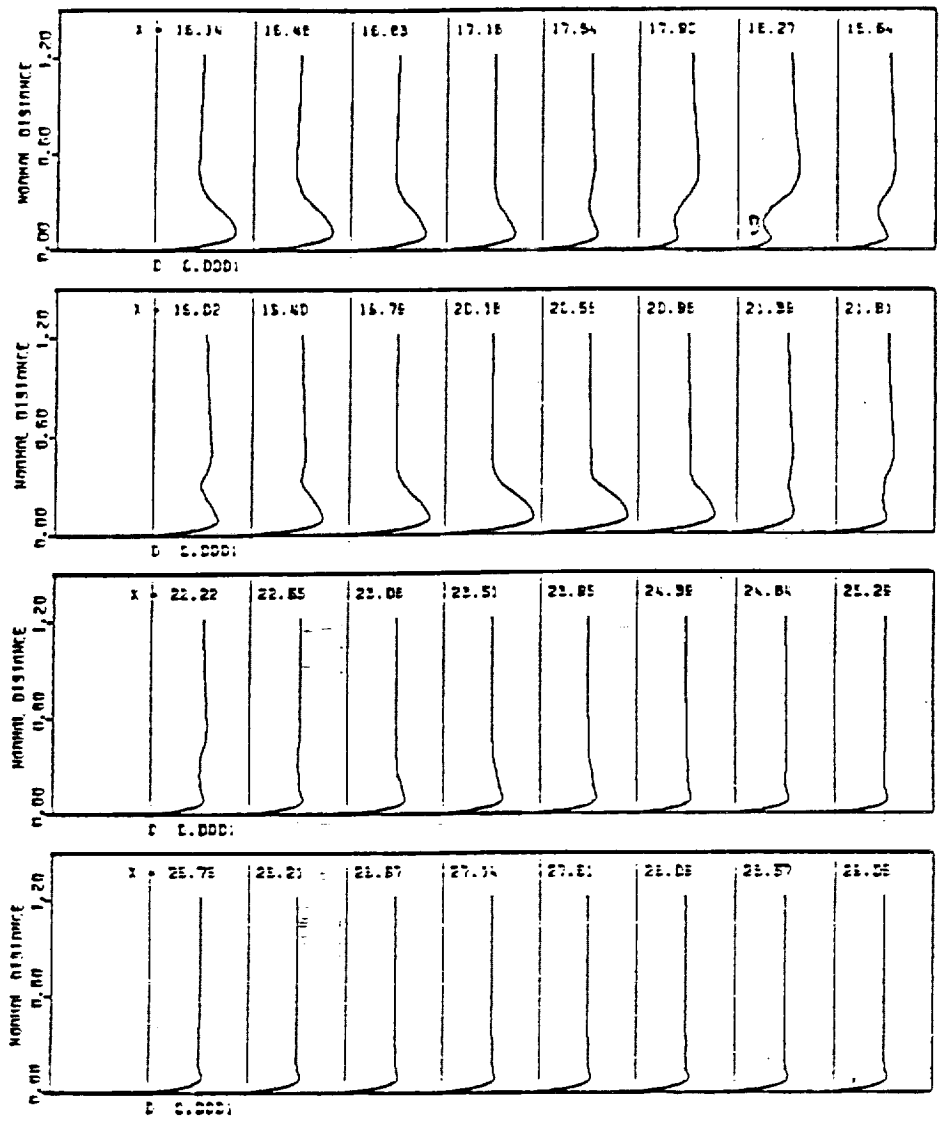


Figure 19a. Continued.

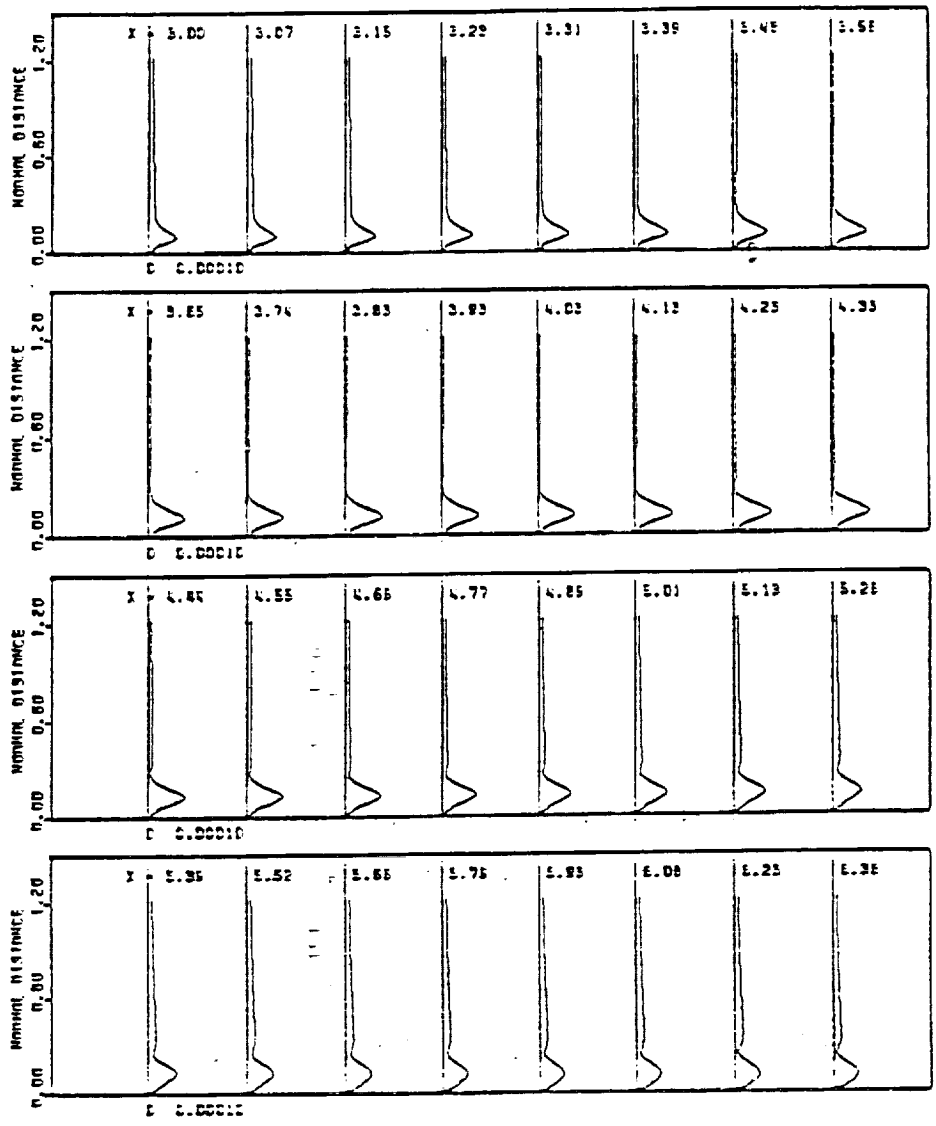


Figure 20. Amplitude profiles of streamwise perturbation velocity u' taken during the fifth cycle at consecutive downstream locations after the Stokes wave is subtracted; F = 230, $a_0$ = 0.0001.

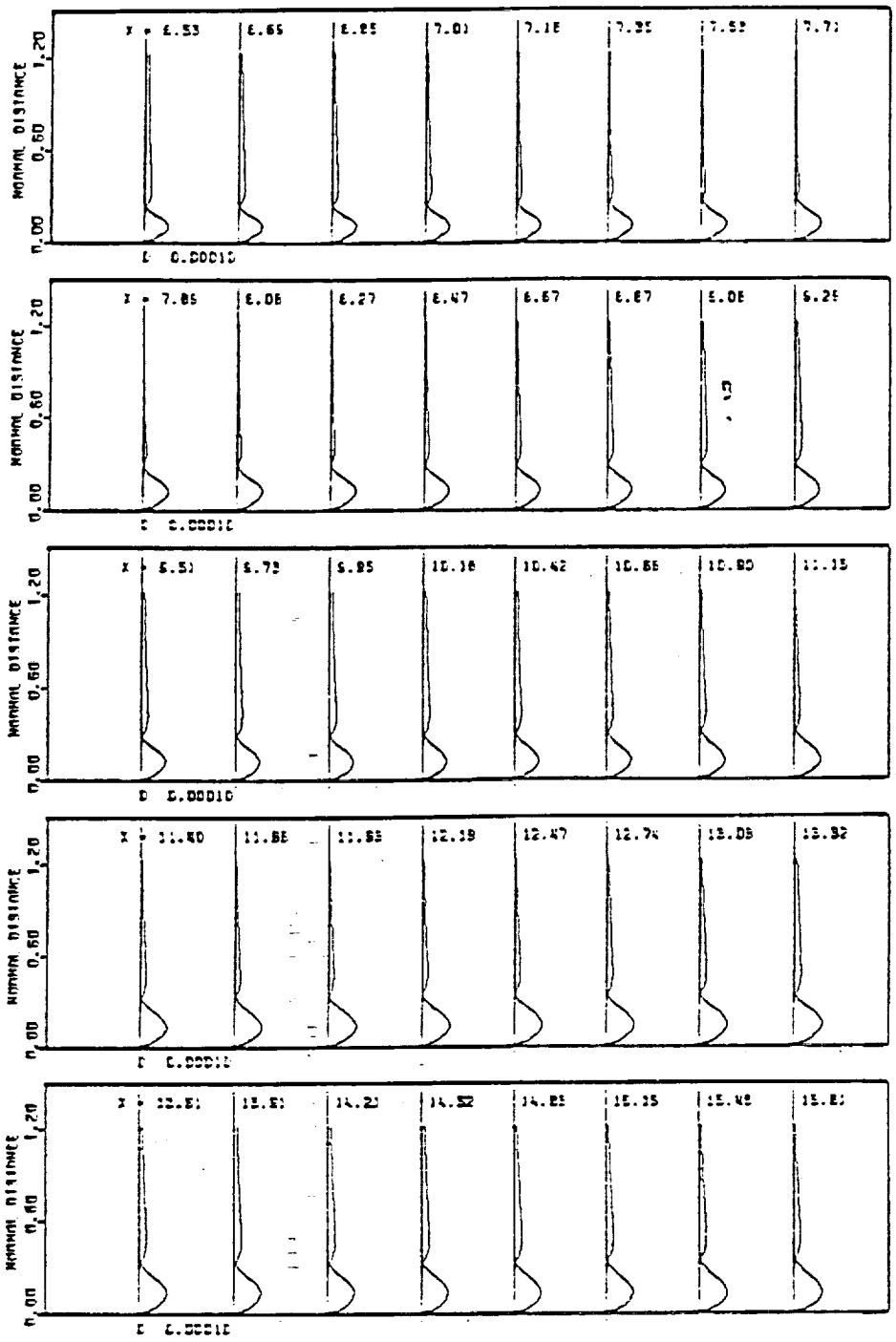


Figure 20a. Continued.

ORIGINAL PAGE IS
OF POOR QUALITY

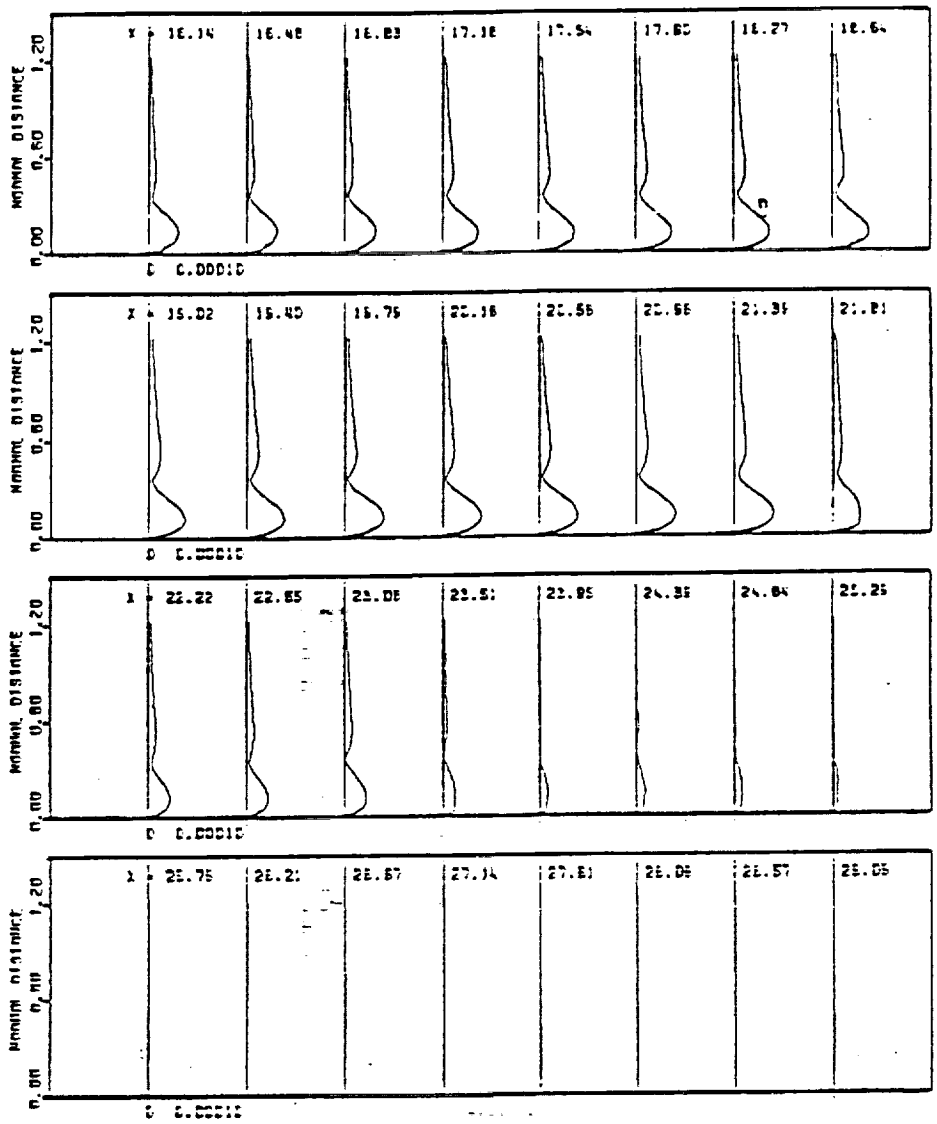


Figure 20a. Continued.

Figure 21 Basic-state C-type grid for the swept wing.

(a)

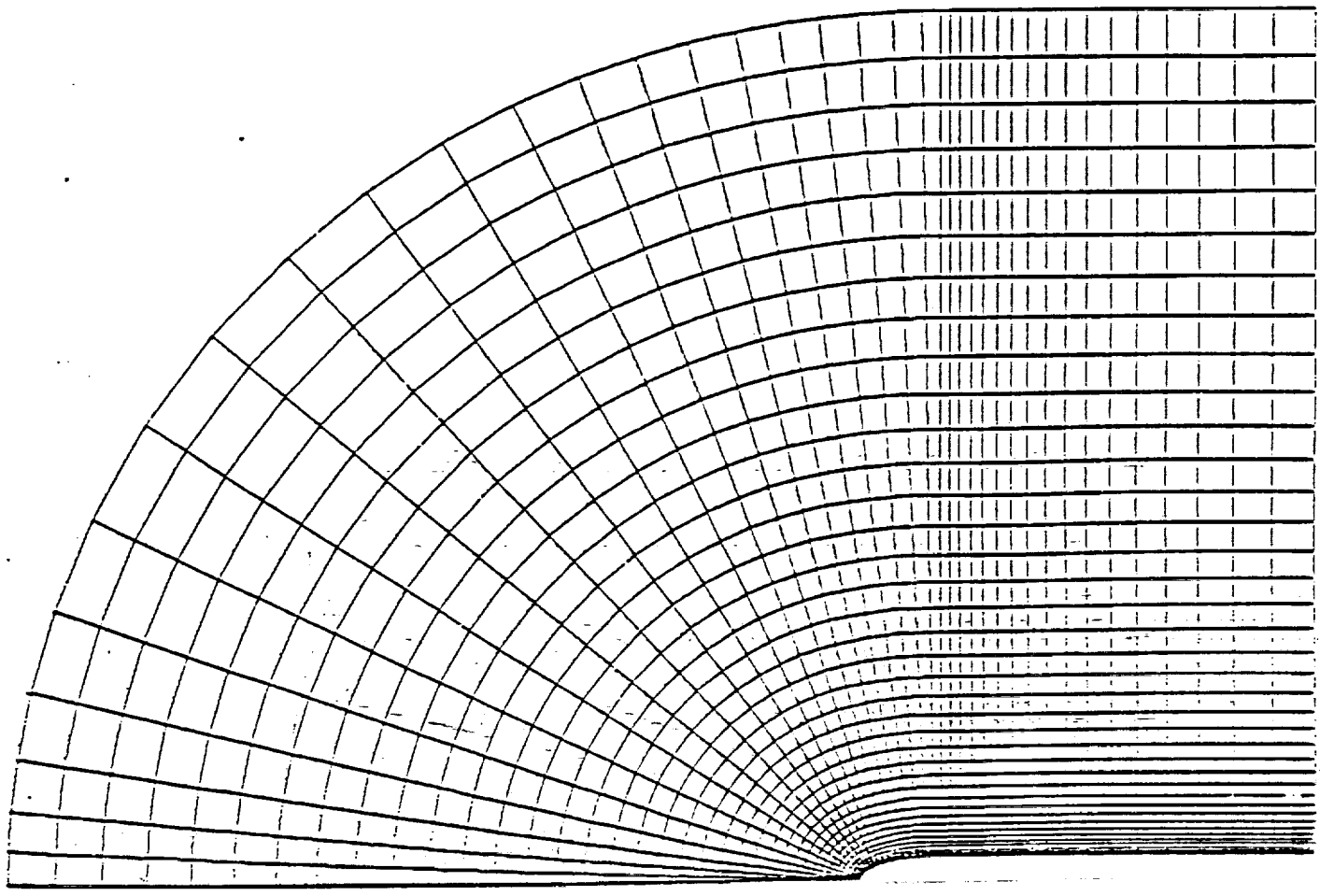

GRID : 39 BY 40

MINIMUM I-SPACING AT L.E. :0.005702

MINIMUM I-SPACING AT L.E. :0.000788

(b)



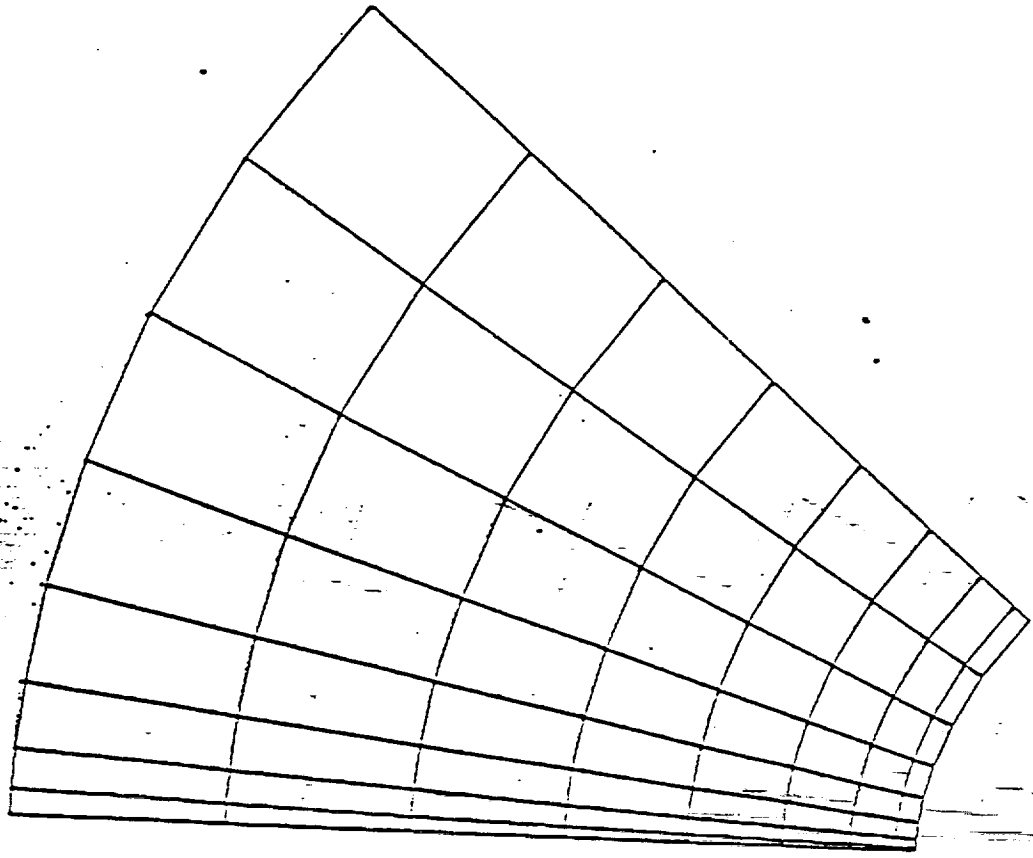

Blown-up View at Leading Edge

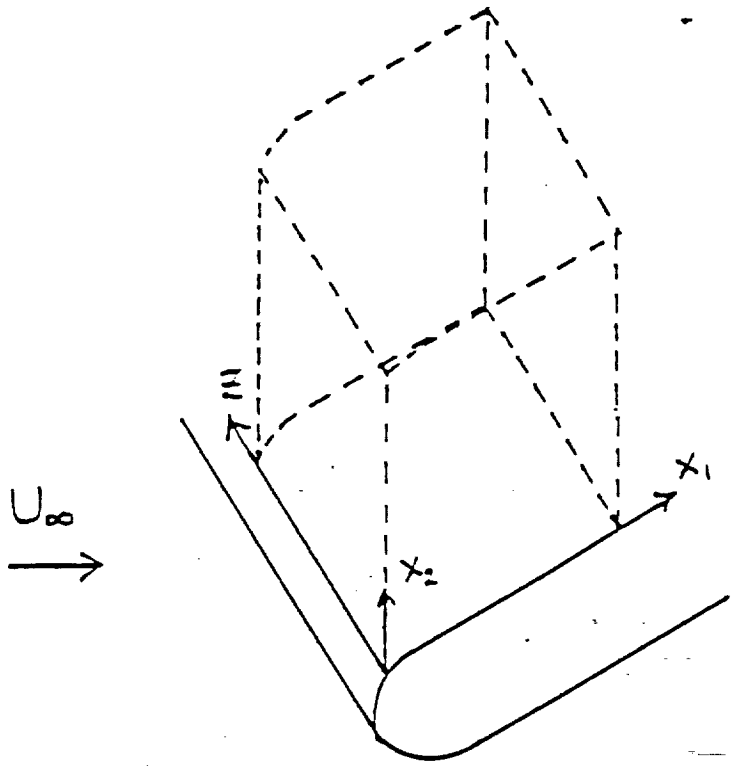


Figure 22. Computational box for the swept wing, with upstream end close to the leading edge and downstream end in the zero-pressure-gradient region in mid-chord to allow for crossflow/TS interactions, is fixed to the surface (*spatial simulation*).

Figure 23a Typical results of the solution of the *three-dimensional basic state* for a sweep angle of 23 degrees and a Reynolds number based on nose radius of 1000 are presented here for Configuration 1. The pressure coefficient distribution is shown from our Navier-Stokes calculations. $C_p$=1 corresponds to the stagnation point.

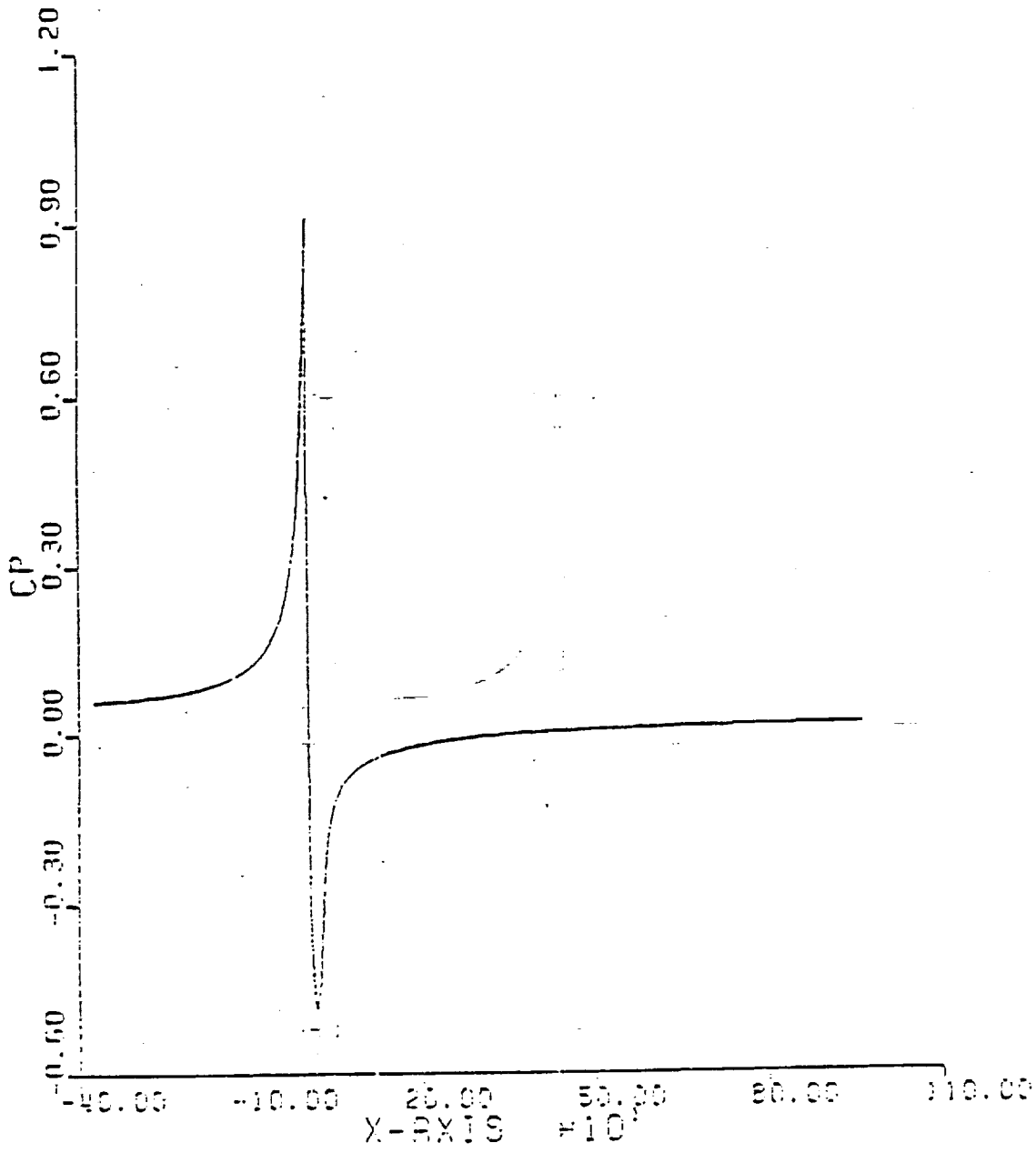

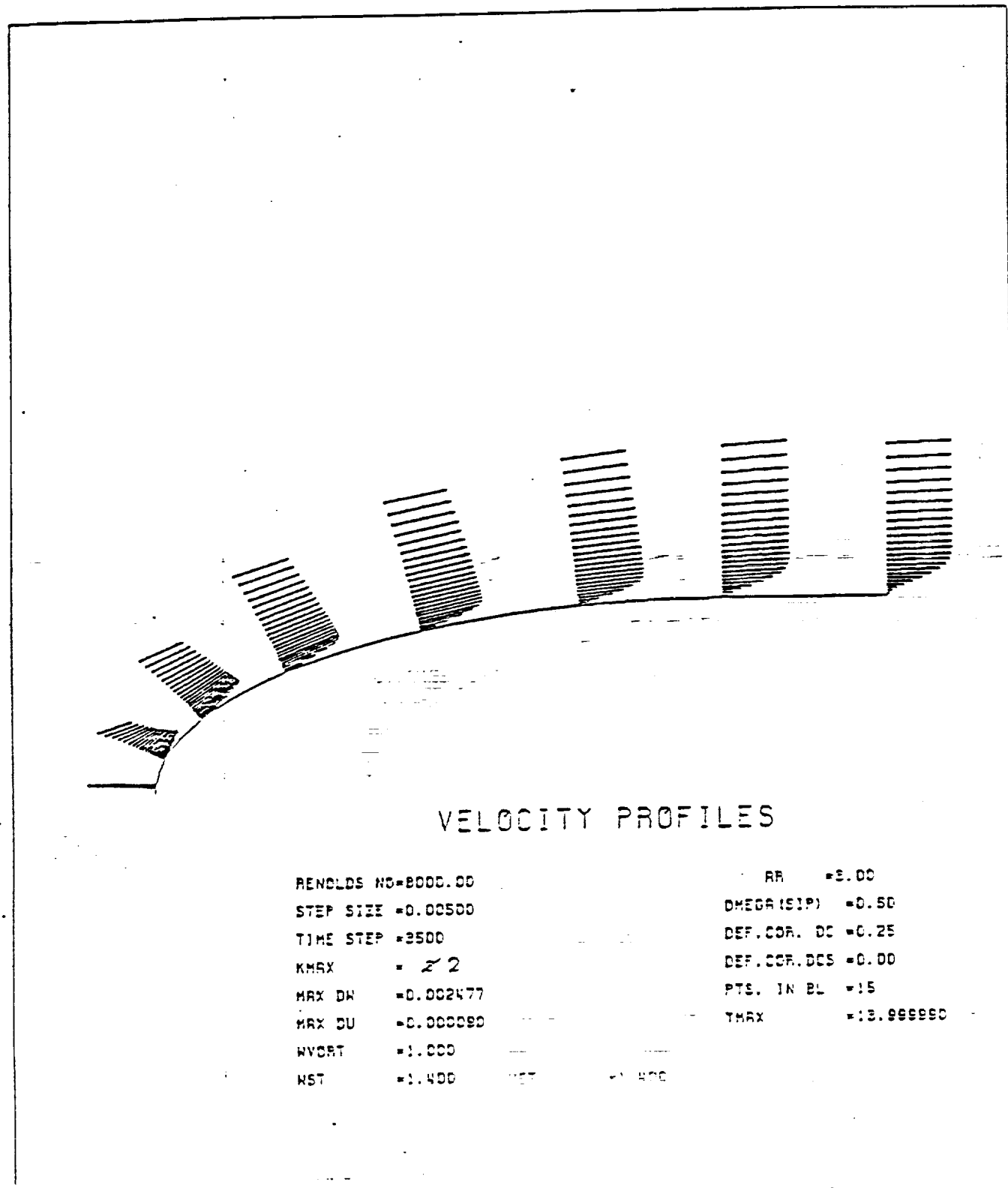


Figure 23b Typical chordwise (perpendicular to the leading edge) profiles are shown from our Navier-Stokes calculations.

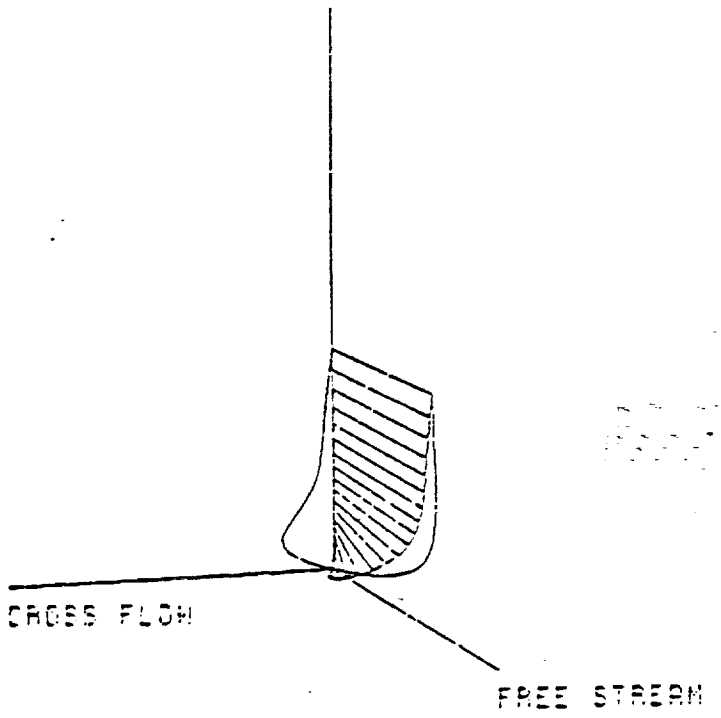


Figure 23c Typical crossflow profiles are shown from our Navier-Stokes calculations.

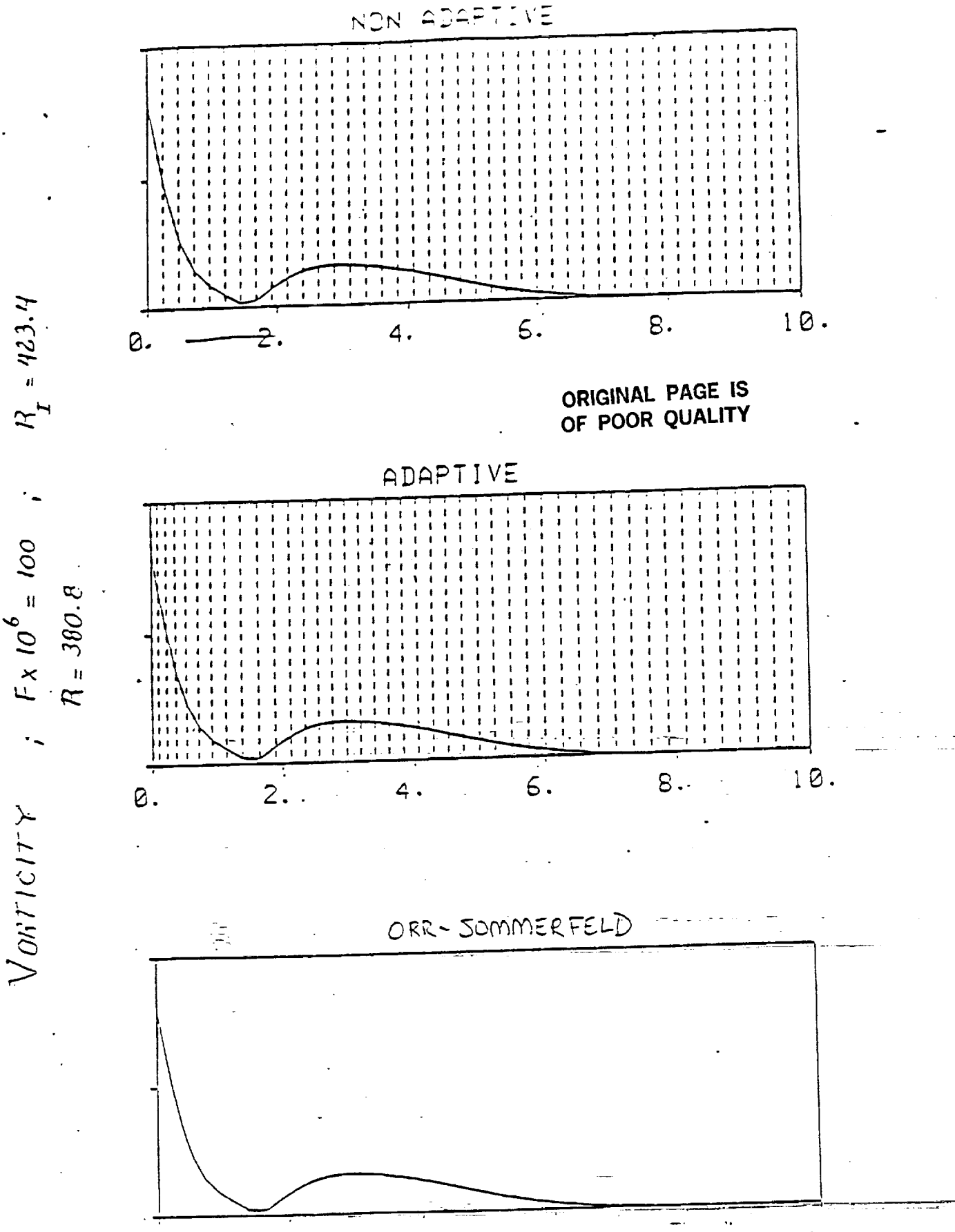


Figure 24 Considering the two-dimensional basic state (that is, the sweep angle is zero) and introducing unsteady disturbances at the leading edge yields the following results. For a nondimensional frequency of F = 100 * 10-6, we show the spanwise disturbance vorticity by a) our Navier-Stokes code with a uniform grid, b) our Navier-Stokes code with grid adaption, and c) an Orr-Sommerfeld solution. As expected, the comparison is good.

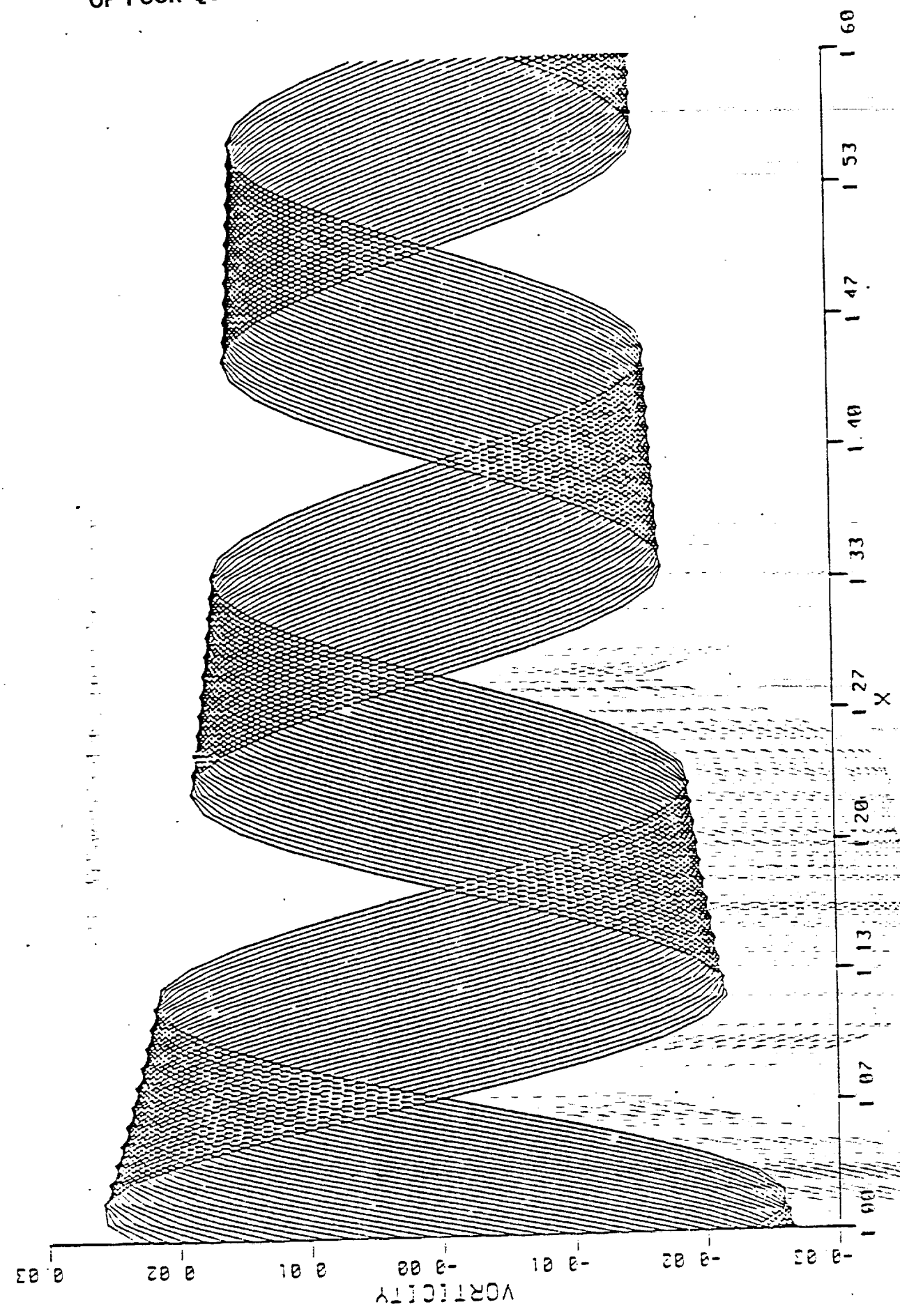


Figure 25 Wall-vorticity distribution with downstream distance for various times.

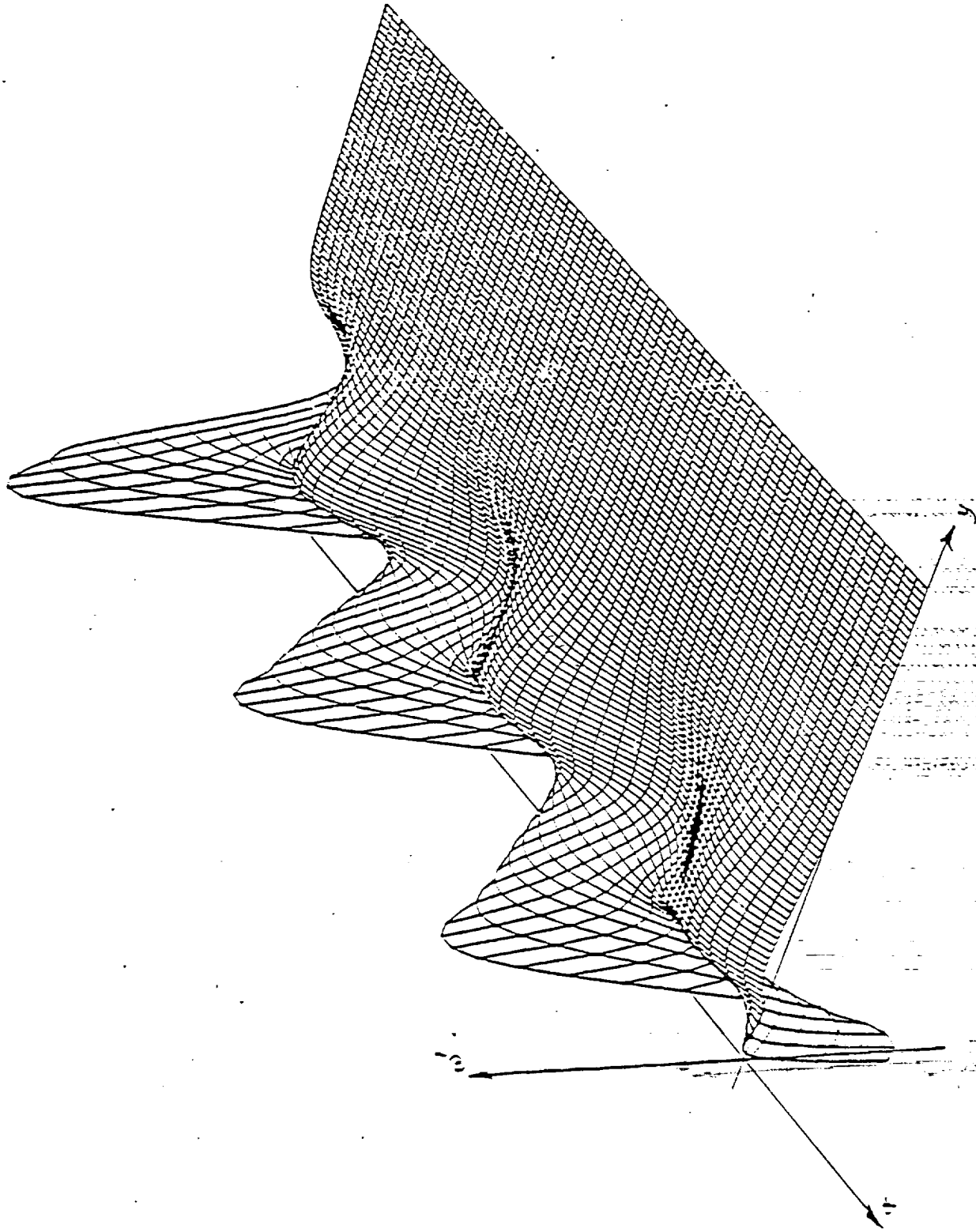


Figure 26 Vorticity disturbance amplitude distribution with downstream distance. Again, the shapes and growth rates compare very well with Orr-Sommerfeld theory.

Figure 27 Streamwise velocity disturbance amplitude distribution with downstream distance. Again, the shapes and growth rates compare very well with Orr-Sommerfeld theory.

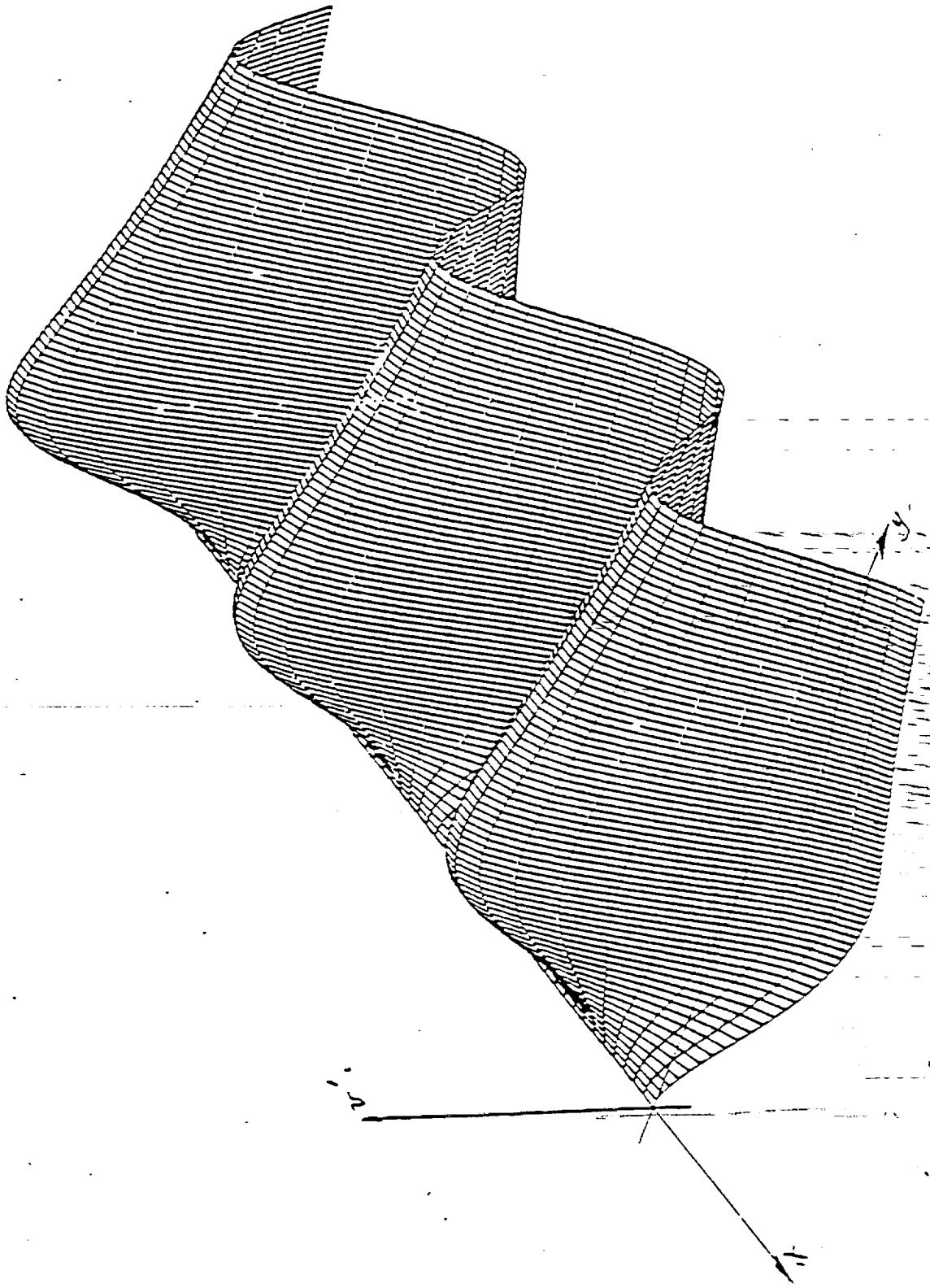

Figure 28 Normal velocity disturbance amplitude distribution with downstream distance. Again, the shapes and growth rates compare very well with Orr-Sommerfeld theory.

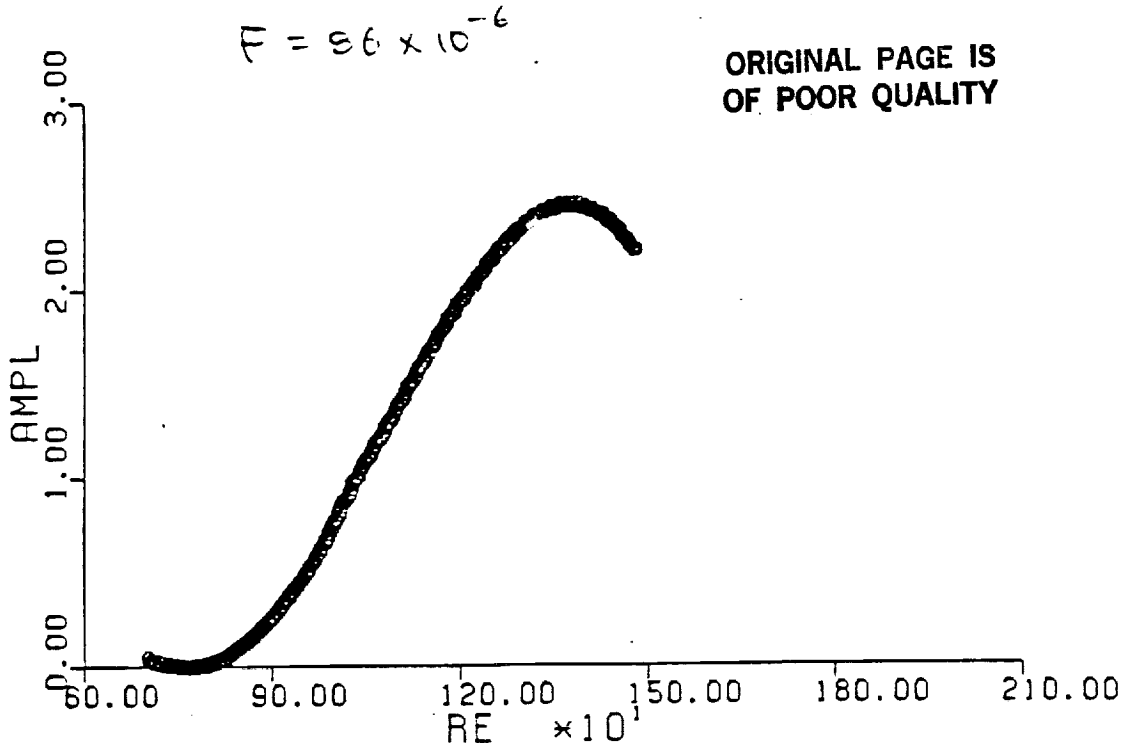


Figure 29 Typical N-factor curve for the two-dimensional basic state for comparison with Figure 30. Here F = 86 * 10-6. We see that the neutral points are accurately predicted. Based on these results, we are very encouraged about our numerical methods.

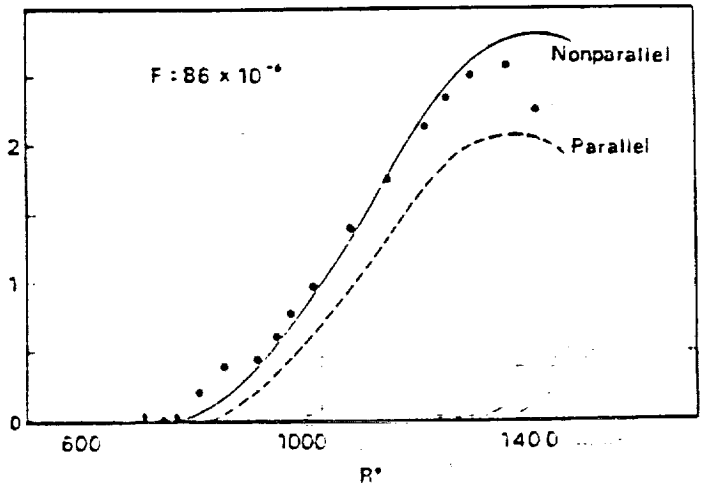


Figure 30 N-factor curve from Saric & Nayfeh (1977) for F = 86 * 10-6. This is a copy of their Figure 8.

NASA
FORMAL
REPORT

FFNo 665 Aug 65